University of Alberta
Printing Department

THE UNIVERSITY OF ALBERTA

INVESTIGATION OF A MICROWAVE LUNEBERG LENS

A THESIS

SUBMITTED TO THE FACULTY OF GRADUATE STUDIES

IN PARTIAL FULFILMENT OF THE REQUIREMENTS FOR THE

DEGREE OF MASTER OF SCIENCE

DEPARTMENT OR DIVISION OF ELECTRICAL ENGINEERING

by

George Bidulock

EDMONTON, ALBERTA

APRIL 1, 1960

UNIVERSITY OF ALBERTA

FACULTY OF GRADUATE STUDIES

The undersigned certify that they have read, and recommend to the Faculty of Graduate Studies for acceptance, a thesis entitled,"Investigation of a Microwave Luneberg Lens", submitted by G. Bidulock in partial fulfilment of the requirements for the degree of Master of Science.

ABSTRACT

Since materials with continuous variation of refractive index are unavailable for spherical Luneberg lens construction, an investigation is made of a stepped-index, spherically symmetrical lens constructed by stacking 19 one-half inch Perspex discs, of varying diameter, to form a 10-inch sphere. Refractive index is varied by machining cylindrical voids in each one-half inch annulus of each disc.

The Clausius-Mossotti equation is used to determine the number and size of voids required. The exactness of this relationship is checked by dielectric constant measurements on a perturbed dielectric using the shorted-waveguide method of measurement. Complete lens design tables are given.

The Luneberg lens was tested at X-band frequencies. The resultant radiation patterns are shown and compared to the theoretical diffraction pattern developed for a circular aperture of similar dimensions. Other variables tested,far-field distance, feed-horn alterations, focusing ability and defocused radiation patterns, and lens gain, are also discussed.

ACKNOWLEDGEMENTS

The author wishes to acknowledge the helpful criticism of Professor J.W. Porteous toward both the testing methods and the preparation of the thesis.

Gratitude is expressed to Willis Plastic Signs of Edmonton, Alberta, for providing the Perspex sheet at a reduced price, and to F.G. Szojka for his assistance in taking the photographs.

TABLE OF CONTENTS

TABLE OF CONTENTS

LIST OF TABLES

LIST OF FIGURES GRAPHS AND ILLUSTRATIONS

LIST OF FIGURES GRAPHS AND ILLUSTRATIONS

CHAPTER I INTRODUCTION

1.1. INTRODUCTORY REMARKS

This presentation considers the theory, design, construction and testing of a spherically symmetrical microwave lens of the Luneberg type. Following these remarks is a brief review of microwave lenses followed by a general discussion of the Luneberg lens. The equations related to this topic are derived in Chapter II. Chapters III and IV present the design, construction and measurement of the lens with concluding remarks given in Chapter V.

The increased use of wavelengths in the micrwave region has necessitated the design of radiating systems closely related to optical devices. Radio frequency systems have radiators of size comparable to one wavelength of the radiated field. The directivity of these devices is controlled by the phase and amplitude of currents flowing in conducting radiating elements. Extrapolation of this method into the microwave region is difficult because of the following reasons.

At centimeter wavelengths waveguides rather than open-wire or coaxial type of feeder lines are used. The radiated pattern must approach a searchlight type shape to help fulfill the desired function of the equipment feeding into the radiating system. The emitted wavelength is usually much smaller than the practical dimensions of the radiating system.

Since an open-ended waveguide acts similarly to an optical point source and since the desired system characteristics approach the characteristics of an optical system, it is more convenient to design microwave radiating systems using optical theory rather than the familiar applications of currents flowing in conducting elements.

As has been mentioned, an open-ended waveguide behaves like a point source radiator. This seems to be a good starting point for the system design. The primary pattern radiated by the point source may be collimated into a searchlight type beam by use of an appropriately shaped reflector. The spherical phase-fronts (wavefronts over which the phase of the electromagnetic field is constant) from the open-ended waveguide are changed into plane phase-fronts of a searchlight type beam.

The system described, based on the reflective laws of optics, has two main disadvantages. First, the open-ended waveguide or horn, which must be located at or near the focal point of the reflector surface, interfers with the secondary pattern produced by the reflector. Secondly, for good reflection the reflector surface must be constructed of a conducting sheet or mesh held into shape by a framework. The aperture or cross-sectional dimensions of the reflector must be sufficiently large to minimize diffraction effects and to allow enough energy to be received at the horn. The reflector alone may weigh from a few hundred pounds to several tons. In a scanning action the radiating system must

be rotated. Thus, for radar applications, a great deal of power must be used to rotate the reflector.

These difficulties, encountered in a source-reflector system, can be at least partially overcome by using a source-lens system dependent on the refractive laws of optics. The lens may be constructed from metal plates or plastic dielectrics and would focus the spherical phase-fronts from the source into plane phase-fronts. If the lens possesses cylindrical or spherical symmetry, revolution of the source alone about the lens provides a 360° scan.

1.2. REVIEW OF MICROWAVE LENSES

The study of microwave lenses can be traced back to James Clerk Maxwell in 1854. Sir Oliver Lodge in 1889 demonstrated the focusing ability of a tar lens by showing its beaming effect on the radiation from a spark-gap oscillator. Perhaps the most significant development in this field came just after World War II when higher frequency sources became available. Artificial dielectric materials, constructed of metal plates, rods, spheres and discs, were developed[1] and thus a host of new materials became available for lens construction.

The refracting media from which lenses can be constructed may be classified as:-

1. solid dielectrics,
2. metallic delay dielectrics,

3. path length dielectrics,

4. metal-plate or rodded dielectrics.

Solid dielectric lenses behave in a way similar to the transparent materials used in optical work. Such lenses are constructed by machining a block of dielectric to the required profile.

The metallic delay dielectric represents a large scale model of a molecular structure and behaves like a solid dielectric. Metallic discs or spheres arranged in a cubic array provide an effective dielectric with an index of refraction greater than unity.

Path length dielectrics may be constructed from inclined, corrogated or curved metal plates. The electric field vector is perpendicular to the plates and the spacing between plates is less than one-half wavelength. Hence different portions of the primary wave-front are caused to travel different distances so that the emerging wave-front is plane. The phase velocity within the lens is constant.

Metal-plate and rodded dielectrics depend on the fact that the phase velocity between parallel conducting plates or rods is greater than the free-space velocity, when the electric field is parallel to the plates or rods. Spacing between the plates is usually between one-half and one wavelength. The refractive index of this dielectric is less than unity.

Representative convex lenses using the dielectrics outlined, are pictured in Figure (1.1). Since the index of

refraction of a metal-plate dielectric is less than unity, a concave shape is required to provide a convex type of focusing.

Microwave lenses may also be classified as homogeneous or inhomogeneous. Homogeneous lenses are characterized by the fact that the dielectric medium used has a constant index of refraction. Focusing, in these lenses, is accomplished by varying the shape of the lens profile.

The most important inhomogeneous microwave lenses are those in which the index of refraction varies with radius only. These lenses have been investigated by several authors.[2 - 7] The classical work of Luneberg[8] has brought additional attention to the subject with regard to wide-angle scanning microwave applications.

1.3. THE LUNEBERG LENS

Luneberg[8] has developed the theory for spherically symmetrical lenses whose index of refraction varies with radius only. These lenses image all points of one sphere perfectly on another concentric sphere. As a special case, the radius of one sphere is taken as unity and the radius of the other is infinite. The resultant lens is referred to as the Luneberg lens. It has the property of collimating a plane phase-front into a point on the surface of the lens as shown in Figure (1.2). In this diagram, the following advantages of this lens, used as a wide-angle microwave

(a) Solid Dielectric lens

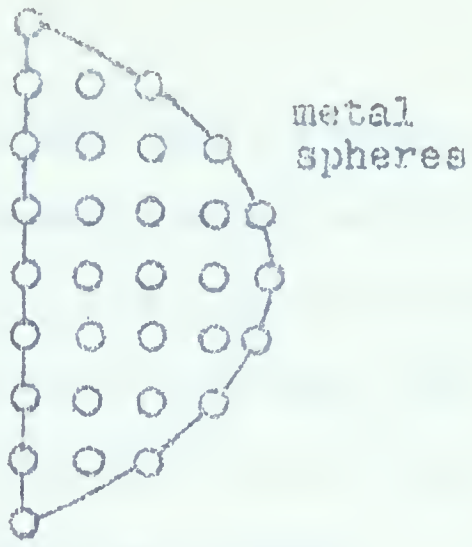

(b) Metallic Delay lens

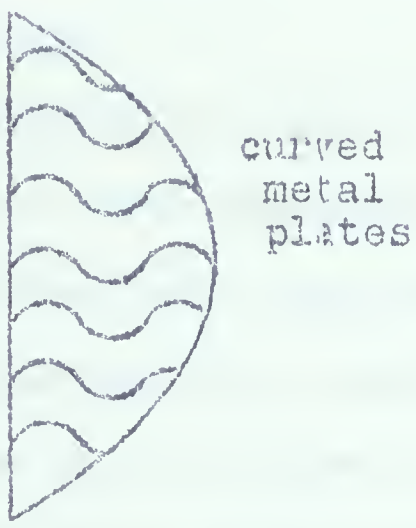

(c) Path Length lens

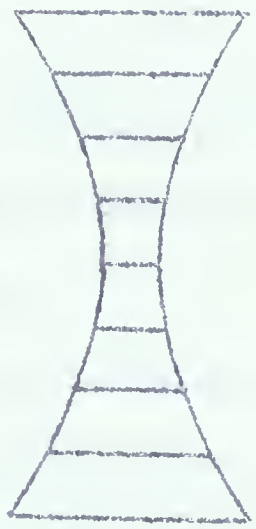

(d) Metal-plate lens

Fig. 1.1 - Homogeneous Microwave lenses.

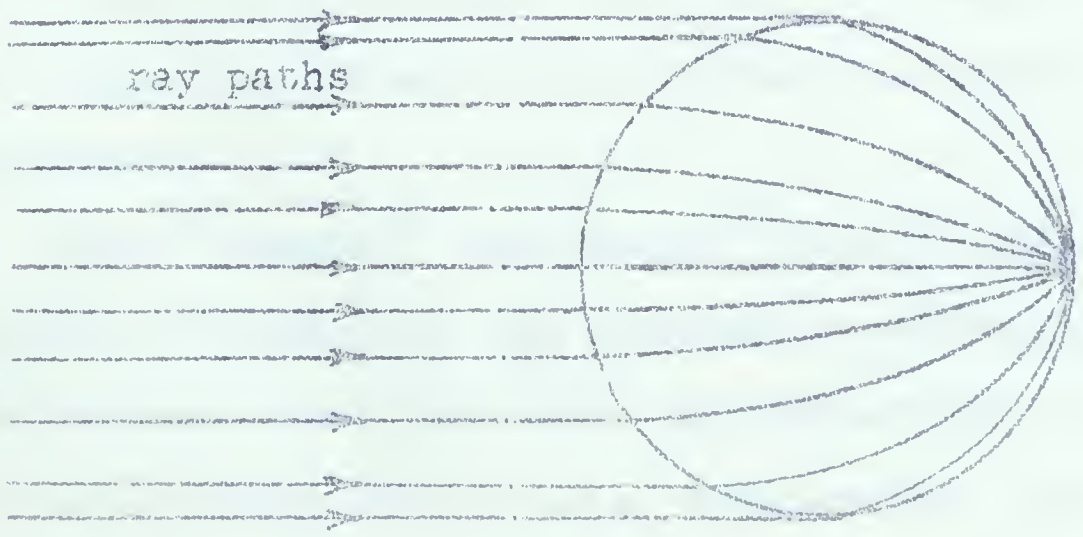

Fig. 1.2 - The Luneberg lens.

scanner, are indicated.

1. The complete aperture of the lens is used.
2. The source alone moves about the circumference of the lens, thus reducing the required torque.
3. Scan can be performed not only through 360° in azimuth but also through 180° in altitude.
4. The index of refraction at the surface of the lens is unity thus providing no lens-to-air discontinuity and hence a minimum of reflections occur.
5. Encasing the lens in a metallic hemispherical shell provides a wide-angle reflector with a narrow beam characteristic.
6. Theoretically, neglecting diffraction effects, the lens produces a parallel-sided beam of diameter equal to the diameter of the lens.

Although the advantages mentioned would indicate that this lens is a perfect instrument for radar applications, a lens of suitable size would be about six feet in diameter and the torque requirement for rotating the source would be appreciable.

Brown,[9] Gutman,[10] and Morgan,[11] have developed mathematical solutions to the problem by developing a modified Luneberg lens for which the feed-circle lies inside the periphery of the lens. Furthermore, Kay,[12] in an attempt to reduce feed-circle diameter, as well as provide a spherical cavity at the center of the lens for microwave

components, has shown that a modification which causes the feed-circle to lie within a cavity at the center of the lens, is impossible. Satisfactory solution of the feed-circle problem usually causes an increase in mechanical complexity.

Other applications for modified Luneberg lenses have been developed by Huynen.[13] The cases of focusing a conical wave into a point opposite to the point of entry of the wave, transforming an incoming plane or conical wave into an outgoing conical or plane wave with arbitrary cone angle, and focusing a curved symmetrical wavefront into a point opposite to the point of entry, are discussed.

Construction of a Luneberg lens for optics has been prohibited by the impossibility of controlling the refractive index of optical materials. Until recently, only two-dimensional models of microwave Luneberg lenses had been constructed from the metallic dielectrics discussed earlier. More recently, Peeler and Coleman[14] successfully constructed a stepped-index spherically symmetrical model using spherical shells molded from expanded polystyrene materials.

The Luneberg lens constructed for this presentation is a stepped-index, spherically symmetrical model using flat Perspex discs of varying diameter. The discs are stacked to form an approximately spherical shaped lens.

CHAPTER II MATHEMATICAL FORMULATION

2.1. THE LUNEBERG LENS EQUATION

In the development of the equation for the required variation of index of refraction with radius for the Luneberg lens, use is made of Fermat's Principle and the Euler-Lagrange equation from variational calculus. Fermat's Principle states that a light ray is a curve along which the time required for the light to travel, is a minimum. The equation for the ray path is minimized by use of the Euler-Lagrange equation.

Luneberg's result can be demonstrated by the following more direct approach applicable to the single case where one focal point is at infinity while the other is at the surface of the spherical lens. If the index of refraction, n, is defined as the ratio of the speed of the wave in vacuum, c, to its speed within the medium, v, then the path length of a ray is given by

$$R = \int n\,ds = c\int \frac{ds}{v} = c\int dt$$

where R is the path length and ds is an element of path length.

Consider now a light ray traveling from point P_1 to P_2 in a medium where n varies with radius (see Figure 2.1). By Fermat's Principle

$$dR = n\,ds = \frac{n\,dr}{\cos\phi} = \frac{nr\,d\theta}{\sin\phi} = f\left(r, \frac{dr}{d\theta}\right)d\theta \qquad (2.1)$$

where $ds\cos\phi = dr$ and $ds\sin\phi = r\,d\theta$

Minimizing equation (2.1) by the Euler-Lagrange equation given by

$$k = f - \frac{dr}{d\theta}\frac{\partial f}{\partial r}$$

gives a generalized form of Snell's law

$$k = nr \sin\phi \qquad (2.2)$$

where k is a constant along any ray path.

Combination of equations (2.1) and (2.2) results in two seperate equations, one giving the path length between two points and the other giving the angle from the origin to a point on the ray for a particular set of values for r, n and k. These two equations are

$$R = \int_{P_1}^{P_2} \frac{n\,dr}{\cos\phi} = \int_{P_1}^{P_2} \frac{n^2 r\,dr}{\sqrt{n^2r^2 - k^2}} \qquad (2.3)$$

$$\theta = \int_{P_1}^{P_2} d\theta = \int_{P_1}^{P_2} \tan\phi\,\frac{dr}{r} = k\int_{P_1}^{P_2} \frac{dr}{r\sqrt{n^2r^2 - k^2}} \qquad (2.4)$$

Consider now the case of the Luneberg lens shown in figure (2.2). In this diagram, the minimum radius to the ray path is given as r_o and the corresponding angle is θ_o. This point on the ray path, P_o, is called the turning point. On either side of the turning point, r increases and the ray path possesses symmetry about the radial line r_o. At the turning point, from equation (2.2), $k = nr_o$ since $\phi = 90^o$ at this point. At the turning point integrals of equations (2.3) and (2.4) are infinite because of the vanishing of the denominators of the

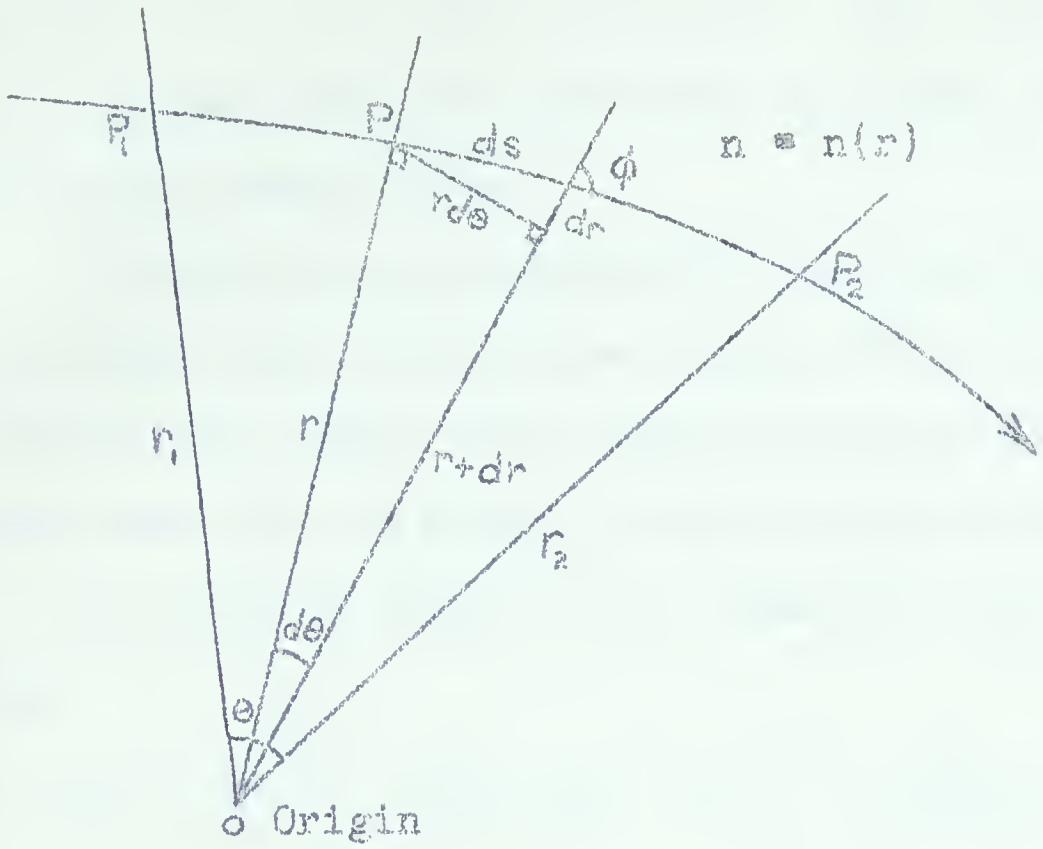

Fig. 2.1 - Ray path geometry.

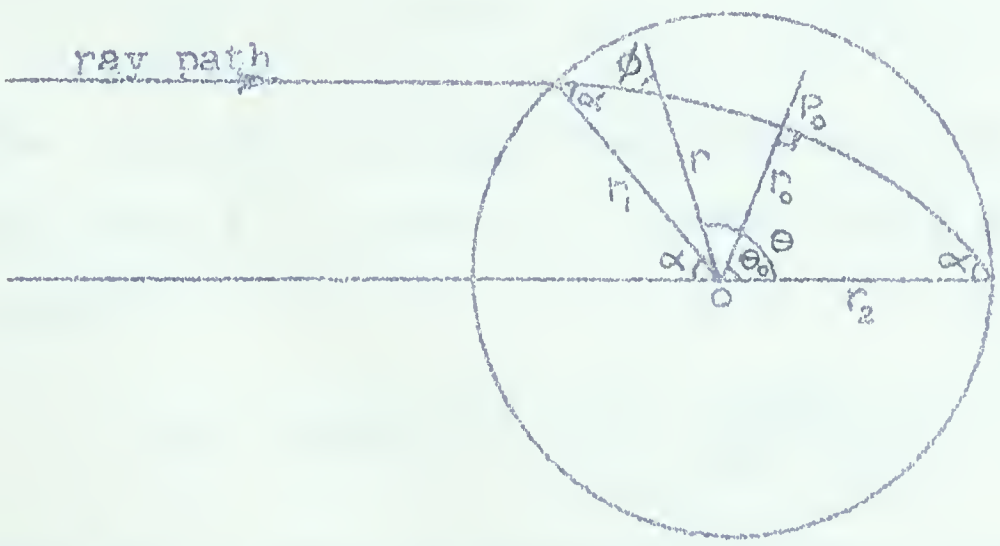

Fig. 2.2 - Luneberg lens ray path geometry.

integrands. To avoid this singularity, the integration range is divided into two segments, one above the turning point and the other below.

It will now be convenient to use the expression $\rho = nr$ since this combination occurs often. Furthermore, the actual path length that the wave travels is not of interest here. Use is made of equation (2.4) only.

In view of Figure (2.2), equation (2.4) can be written

$$\Theta = \pi + k\int_{\infty}^{1} \frac{dr}{r\sqrt{\rho^2 - k^2}} - 2k\int_{r_o}^{1} \frac{dr}{r\sqrt{\rho^2 - k^2}} \qquad (2.5)$$

Outside the boundary of the lens, the index of refraction is unity, hence, $n = 1$, $\rho = r$ and $k = r \sin \phi$. Evaluation of the first integral on the right hand side of equation (2.5) is possible and (2.5) then becomes,

$$\Theta = \pi - \arcsin k - 2k\int_{r_o}^{1} \frac{dr}{r\sqrt{\rho^2 - k^2}} \qquad (2.6)$$

The ray path intersects the positive side of the axis at the point $r = 1$ and $\theta = 0$. Hence r must satisfy the equation

$$\pi = \arcsin k + 2k\int_{r_o}^{1} \frac{dr}{r\sqrt{\rho^2 - k^2}} \qquad (2.7)$$

This is an integral equation for the function ρ . The evaluation of the integral in this equation is difficult but by a series of changes of variable and the application of a known formula, this equation can be solved for the index of refraction as a function of the radius.

If $\tau = \log r$ and $\Omega(\rho) = -\log r(\rho)$, the integral term in equation (2.7) can be written in the following sequence

$$f(K) = K\int_{r_0}^{1} \frac{dr}{r\sqrt{\rho^2 - K^2}} = K\int_{-\infty}^{0} \frac{d\log r}{\sqrt{[\rho(\log r)]^2 - K^2}}$$

$$= K\int_{-\infty}^{0} \frac{d\tau}{\sqrt{[\rho(\tau)]^2 - K^2}} = -K\int_{K}^{1} \frac{d\Omega(\rho)}{\sqrt{\rho^2 - K^2}} \qquad (2.8)$$

The last integral is an integral of Abel's type. For this type of integral, the following inversion formula holds.

$$f(K) = -K\int_{K}^{1} \frac{d\Omega(\rho)}{\sqrt{\rho^2 - K^2}}$$

$$\Omega(\rho) = \frac{2}{\pi}\int_{\rho}^{1} \frac{f(K)\, dK}{\sqrt{K^2 - \rho^2}} \qquad (2.9)$$

The inversion formula can be applied to equation (2.7) most conveniently be writing

$$f(K) = \tfrac{1}{2}(\pi - 2\arcsin K) + \tfrac{1}{2}\arcsin K \qquad (2.10)$$

Since

$$\tfrac{1}{2}(\pi - 2\arcsin K) = K\int_{K}^{1} \frac{d\rho}{\rho\sqrt{\rho^2 - K^2}} = K\int_{K}^{1} \frac{d\log\rho}{\sqrt{\rho^2 - K^2}}$$

applying the inversion formula to this equality gives

$$-\log\rho = \frac{2}{\pi}\int_{\rho}^{1} \frac{\frac{\pi}{2} - (2\arcsin K)\frac{1}{2}}{\sqrt{K^2 - \rho^2}}\, dK \qquad (2.11)$$

Now, application of the inversion equations (2.9) to (2.10) results in

$$\Omega(\rho) = \frac{2}{\pi}\int_{\rho}^{1} \frac{\pi/2 - \arcsin K}{\sqrt{K^2-\rho^2}}\,dk + \frac{1}{\pi}\int_{\rho}^{1} \frac{\arcsin K}{\sqrt{K^2-\rho^2}}\,dk$$

$$= -\log\rho + \frac{1}{\pi}\int_{\rho}^{1} \frac{\arcsin K}{\sqrt{K^2-\rho^2}}\,dk$$

In view of the results of equation (2.11), this equation can be rewritten as

$$\Omega(\rho) = -\log\rho + \tfrac{1}{2}\log\rho - \tfrac{1}{2}\int_{\rho}^{1} \frac{dk}{\sqrt{K^2-\rho^2}}$$

$$= -\log\rho + \tfrac{1}{2}\log\rho + \tfrac{1}{2}\log\rho - \tfrac{1}{2}\log\left(1+\sqrt{1-\rho^2}\right)$$

$$= -\tfrac{1}{2}\log\left(1+\sqrt{1-\rho^2}\right)$$

Since $\Omega(\rho) = -\log r(\rho)$ and since $\rho = nr$, substitution and solving for n in the above gives

$$-\log r(\rho) = -\tfrac{1}{2}\log\left(1+\sqrt{1-\rho^2}\right)$$

$$\rho/n = \sqrt{1+\sqrt{1-\rho^2}}$$

$$r^2 = 1 + \sqrt{1-n^2r^2}$$

$$n = \sqrt{2 - r^2} \qquad (2.12)$$

This is the Luneberg lens equation. From this equation it can be seen that the index of refraction at the surface of the lens is unity and the index of refraction at the lens center is $\sqrt{2}$. In this equation, r is the normalized

radius, that is, the maximum radius of the sphere is taken as unity. The result can be generalized for a sphere of any radius.

2.2. INDEX OF REFRACTION DETERMINATION

Before a Luneberg lens can be successfully constructed, the index of refraction of the material used must be accurately known. Furthermore, a method of varying index of refraction must be used. Thus, a method of measurement and control of index of refraction is required. This section gives the mathematical theory of the methods used in the design of the Luneberg lens.

2.2.1. Relation To Dielectric Constant

The index of refraction of a medium was defined as the ratio of the velocity of the wave in free space to the velocity within the medium, that is, $n = c/v$. From the solution of Maxwell's electromagnetic equations for propagation through a medium, it has been found that[15]

$$v = 1/\sqrt{\mu\epsilon}$$

where the permeability μ is given by $\mu = \mu_m \mu_o$ where μ_o is the permeability of free space and μ_m is the relative permeability of the medium based on a free space value of unity, and the permittivity ϵ is given by $\epsilon = \epsilon_e \epsilon_o$ where ϵ_o is the permittivity of free space and ϵ_e is the relative permittivity (also called dielectric constant) of the medium based on a free space value of

unity. The free space velocity is given therefore by

$$c = 1/\sqrt{\mu_o \epsilon_o}$$

and the index of refraction becomes

$$n = c/v = \sqrt{\mu_m \epsilon_e}$$

In the absence of a magnetic medium, $\mu_m = 1$ and the refractive index is given by

$$n = \sqrt{\epsilon_e} \qquad (2.13)$$

Thus a measurement of the dielectric constant of the medium, at the required frequency, provides the refractive index of the medium at that frequency.

In the Luneberg lens, the dielectric constant must vary with radius in a manner given by

$$\epsilon_e = n^2 = 2 - r^2 \qquad (2.14)$$

Equation (2.14) is plotted in Figure (2.3).

2.2.2. Shorted-waveguide Method of Measurement

Dielectric constant may be measured, at microwave frequencies, using one of two methods. The method of Saito and Kurokawa[16] involves shaping the dielectric sample into a cylindrical disc and inserting it into a cylindrical cavity resonator oscillating in the TE_{10p} mode. The dielectric constant is measured from the difference between the axial lengths of the cavity tuned to the same frequency with and without the sample. The dielectric loss is found from the reduction in Q of the cavity when the

sample is inserted.

The shorted-waveguide method that has been used, is described here. This method is due to Roberts and von Hippel.[17] The more specialized development, given here, includes implicitly improvements derived by Dakin and Works,[18] and Bowie and Kelleher.[19] In this method, the dielectric sample is shaped into a solid hexahedron and inserted against a short-circuit in a waveguide operating in the TE_{10} mode. The dielectric constant is measured from the distance from the sample boundary to the nearest voltage standing wave minimum (not within the sample). The dielectric loss may be derived from the reduction in the standing wave ratio when the sample is inserted. Figure (2.4) shows the test conditions and the notation used.

If the waveguide is operating in the TE_{10} mode and λ_g is the wavelength in an air-filled guide,

λ_{gs} is the wavelength in a dielectric-filled guide,

λ_a is the wavelength in air,

λ_s is the wavelength in the medium dielectric,

λ_c is the critical wavelength of the guide given by twice the wide dimension of the guide (2a),

then the air-filled guide wavelength is given by[15]

$$\lambda_g = \frac{\lambda_a}{\sqrt{1 - (\lambda_a/\lambda_c)^2}}$$

More generally, it is also true that the wavelength in a dielectric-filled guide is given by

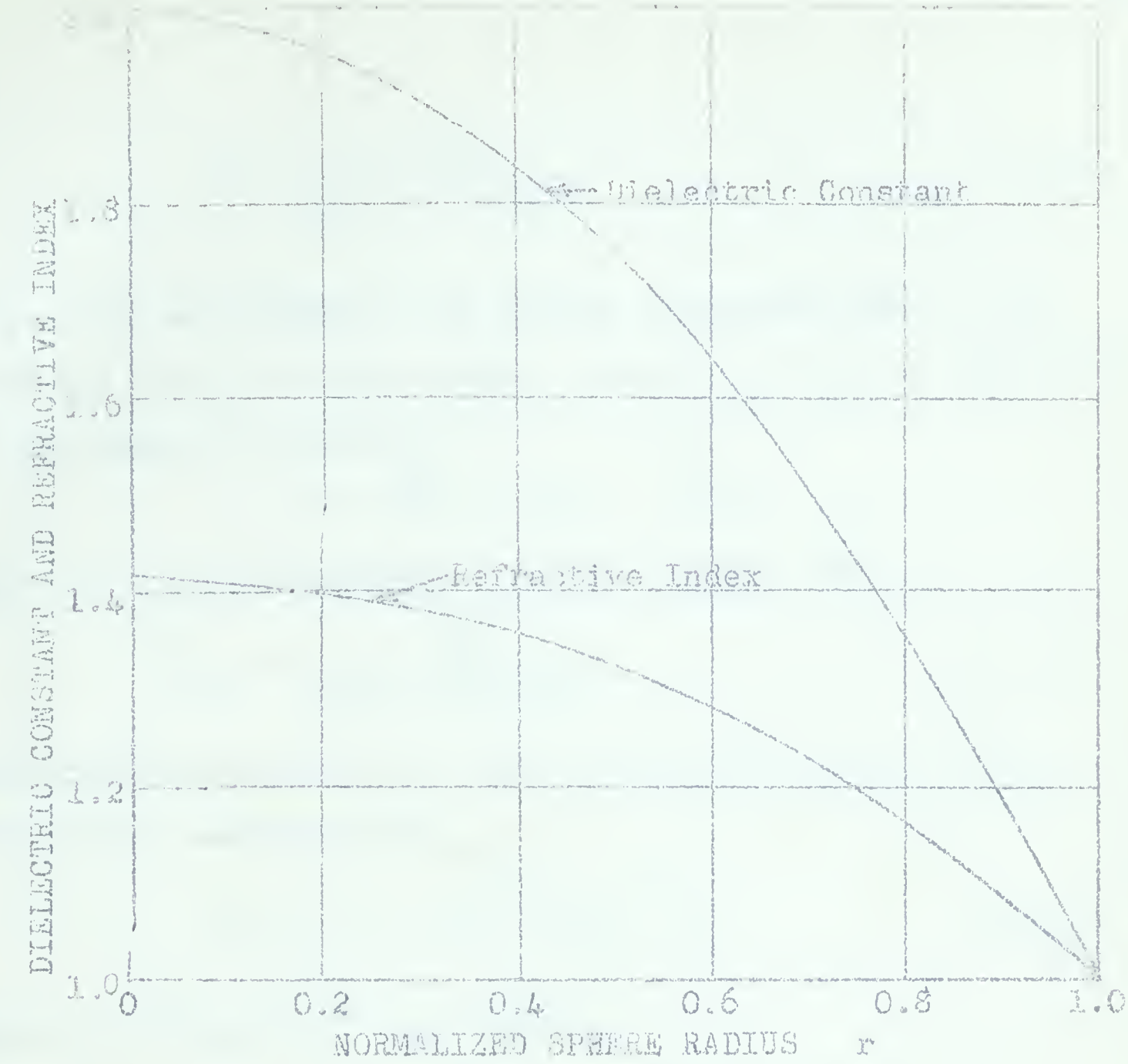

Fig. 2.3 - Dielectric constant and refractive index variations as a function of radius for the Luneberg lens.

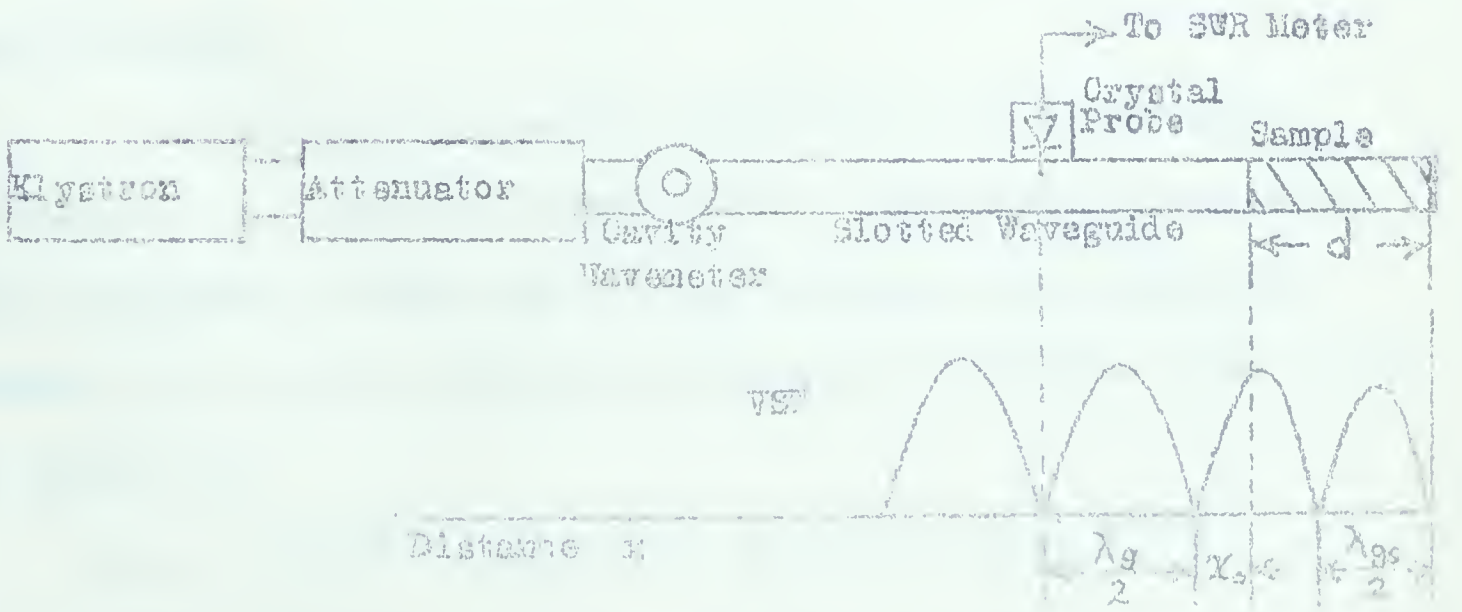

Fig. 2.4 - Shorted-waveguide method for dielectric constant measurement

$$\lambda_{gs} = \frac{\lambda_s}{\sqrt{1 - (\lambda_s/\lambda_c)^2}} \qquad (2.15)$$

Since the wavelength in the medium is proportional to the velocity within the the medium , then the index of refraction of the medium is given by

$$n = \sqrt{\epsilon_e} = c/v = \lambda_a/\lambda_s$$

Equation (2.15) can then be written in the form

$$\lambda_{gs} = \frac{\lambda_a}{\sqrt{\epsilon_e - (\lambda_a/\lambda_c)^2}} \qquad (2.16)$$

Combining equations (2.15) and (2.16) and solving for the dielectric constant gives

$$\epsilon_e = (1-p)(\lambda_g/\lambda_{gs})^2 + p \qquad (2.17)$$

where $p = (\lambda_a/\lambda_c)^2$ = a constant.

The wavelength within the sample in the guide, cannot be directly measured with a slotted line and probe. Thus, this wavelength must be calculated from other measurements.

Consider the sample dielectric in a shorted-waveguide as shown in Figure (2.4). The standing wave in the waveguide is the sum of the incident and reflected waves. At a point x from the dielectric surface, the field is given by

$$E(x) = A_i e^{\gamma x} + A_r e^{-\gamma x} = A_i e^{\gamma x}(1 + r_0 e^{-2\gamma x})$$

$$H(x) = \frac{A_i}{Z_0} e^{\gamma x} - \frac{A_r}{Z_0} e^{-\gamma x} = \frac{A_i}{Z_0} e^{\gamma x}(1 - r_0 e^{-2\gamma x})$$

where A_i and A_r are the amplitudes of the incident and reflected waves respectively, γ is the propagation constant, Z_o is the characteristic impedance of the guide and r_o is the reflection coefficient given by

$$r_o = \frac{A_r}{A_i} = e^{-2\phi} = e^{-2(\rho + j\psi)} = e^{-2\rho} e^{-2j\psi}$$

where $e^{-2\rho}$ is the magnitude and -2ψ is the angle of r_o. For a lossless waveguide, the propagation constant is given by $\gamma = j\beta$

where $\beta = 2\pi/\lambda_g$

The impedance at the point x is given by the ratio of the electric to magnetic fields, $Z(x) = E(x)/H(x)$. At the dielectric face where $x = 0$, the impedance is given by

$$Z(0) = E(0)/H(0) = Z_o \frac{1 + r_o}{1 - r_o} = Z_o \coth \phi$$

Since γ is imaginary, $|e^{\pm \gamma x}| = 1$. The maximum and minimum field amplitudes can be found for the air-filled section of the guide as

$$E_{max} = |A_i||1 + r_o|, \qquad E_{min} = A_i(1 - |r_o|)$$

Their ratio is

$$\frac{E_{min}}{E_{max}} = \tanh \rho$$

At $x = x_o$ there occurs a minimum. Here the incident and reflected waves have a phase difference of π radians. Hence

$$2(\psi + \beta x_o) = \pi$$

and

$$\psi = \frac{\pi}{2} - \frac{2\pi x_o}{\lambda_g}$$

Thus

$$Z(0) = Z_0 \coth \phi = Z_0 \coth(\rho + j\psi)$$

$$= Z_0 \frac{\tanh\rho + \coth j\psi}{1 + \tanh\rho \coth j\psi} = Z_0 \frac{\tanh\rho - j\cot\psi}{1 - \tanh\rho\, j\cot\psi}$$

$$= Z_0 \frac{\frac{E_{min}}{E_{max}} - j\tan\frac{2\pi x_0}{\lambda_g}}{1 - j\frac{E_{min}}{E_{max}}\tan\frac{2\pi x_0}{\lambda_g}}$$

If the loss in the waveguide is considered small, that is, if the dielectric has small loss, then the standing wave ratio will be large and the ratio of the minimum to the maximum fields, may be neglected. The impedance at the dielectric face then becomes

$$Z(0) = -jZ_0 \tan\frac{2\pi x_0}{\lambda_g} \qquad (2.18)$$

In the dielectric, the fields are similarly given by

$$E_s(x) = A_{is} e^{\gamma_s x} + A_{rs} e^{-\gamma_s x}$$

$$H_s(x) = \frac{A_{is}}{Z_{os}} e^{\gamma_s x} - \frac{A_{rs}}{Z_{os}} e^{-\gamma_s x}$$

where Z_{os} is the characteristic impedance of the dielectric-filled guide. At x = -d there exists a short circuit where the electric field is zero. Hence

$$0 = A_{is} e^{-\gamma_s d} + A_{rs} e^{\gamma_s d}$$

and

$$\frac{A_{rs}}{A_{is}} = -e^{-2\gamma_s d}$$

At the face of the dielectric the impedance is then given

by

$$Z(0) = E_s(0)/H_s(0) = Z_{os}\frac{1 + Ars/Ais}{1 - Ars/Ais}$$

$$= Z_s \tanh \gamma_s d$$

For the case of nonmagnetic samples[15]

$$\gamma_s Z_{os} = \gamma Z_o$$

Also assuming low-loss dielectric again, the propagation constant within the dielectric is given by

$$\gamma_s = j\beta_s = j\frac{2\pi}{\lambda_{gs}}$$

The impedance at the face of the sample then becomes

$$Z(0) = \frac{\lambda_{gs}}{\lambda_g} Z_o \tan\frac{2\pi d}{\lambda_{gs}} \qquad (2.19)$$

Equating equations (2.18) and (2.19) for the impedance at the dielectric boundary looking into the dielectric-filled section of the guide and looking into the air-filled section of the guide, results in

$$-\frac{\tan\frac{2\pi x_o}{\lambda_g}}{\frac{2\pi d}{\lambda_g}} = \frac{\tan\frac{2\pi d}{\lambda_{gs}}}{\frac{2\pi d}{\lambda_{gs}}} \qquad (2.20)$$

A method is therefore shown by means of which one may obtain the wavelength within the sample in the guide. Equation (2.17) can then be solved for the dielectric constant of the sample material under test.

The solution of the transcendental equation (2.20) for the wavelength within the sample in the guide is difficult because of the cyclic nature of the tangent function. It is simpler to represent

graphically dielectric constant plotted directly against the ratio x_0/λ_g. Such a graph is shown in Figure (2.5). Here the value of p chosen was 0.50. This value establishes λ_g at 4.70 cms. for an RG-52/U waveguide. Sample lengths of 2.5, 3.0, 5.0 and 6.0 cms. were used.

The cyclic nature of the tangent function introduces ambiguities in the evaluation of the dielectric constant from the graph in Figure (2.5). For one particular value of x_0/λ_g several possible solutions for dielectric constant exist. Use of two different sample lengths will disclose the ambiguities and the correct value of dielectric constant results. Interpolation between curves for intermediate sample lengths is not permitted. Discontinuities exist between curves.

2.2.3. Luneberg Lens Design Equations

Perhaps the simplest method for constructing an artificial dielectric of varying dielectric constant, is one in which a solid dielectric material is perturbed with small discontinuities of different dielectric constant. Variation of the dielectric constant is achieved by varying the density of the perturbations. Artificial dielectrics of this type, (closely related to delay dielectrics discussed earlier) have been constructed and tested.[20,21]

Consider a solid dielectric perturbed by a cubic array of small spherical voids. To predict the resultant dielectric constant of such an artificial dielectric, use

Fig.2.5 - Shorted-waveguide method for dielectric constant measurements.

d = sample length in cms. $p = (\lambda_a/\lambda_c)^2 = 0.50$

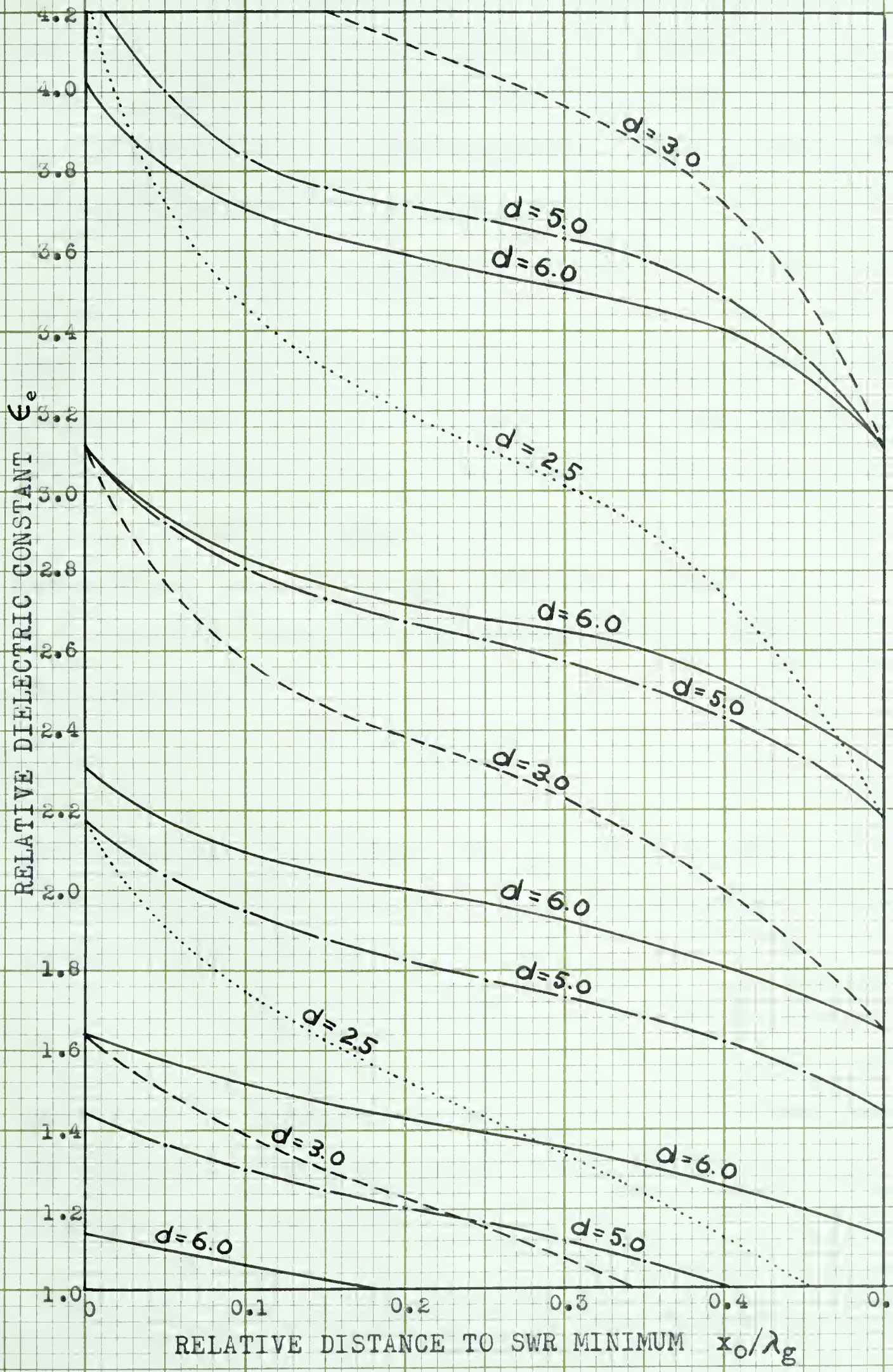

is made of the Clausius-Mossotti relation developed for the case of the dielectric constant of a molecular gas. If the number of gas molecules per unit volume, N/V, and the polarizability, α_e, of these molecules is known, then the Clausius-Mossotti relation predicts that

$$\frac{\alpha_e N}{3V} = \frac{\epsilon_e - 1}{\epsilon_e + 2}$$

The polarizability measures the electrical pliability of the molecules, that is, their ability to form dipoles of increased moment, with increased applied electric field.

In the macroscopic case, the gas molecules are replaced by small spherical voids. The polarizability of a spherical void, in a dielectric medium, is given by the expression[22]

$$\alpha_e = 4\pi R^3\left[\frac{1 - K_1}{1 + 2K_1}\right]$$

where R is the void radius and K_1 is the relative dielectric constant of the surrounding medium. Introducing a fractional volume concept such that

$$f = \frac{\frac{4}{3}\pi R^3 N}{V}$$

where f is the ratio of the void volume, to the volume of the surrounding base dielectric, the Clausius-Mossotti relation can be rewritten

$$\epsilon_e = K_1\left[\frac{1 + 2fC}{1 - fC}\right] \qquad (2.21)$$

where the parameter C is given by

$$C = \frac{1 - K_1}{1 + 2K_1} \tag{2.22}$$

It would appear reasonable to assume that cylindrical voids, of length-to-diameter ratio near unity, would produce the same results as spherical voids of the same volume. For this case, a new fractional volume can be defined to replace the one given for spherical voids. If D is the diameter of the cylindrical void and L is its length, then the fractional volume becomes

$$f_c = \frac{\frac{\pi}{4} D^2 L N}{V} \tag{2.23}$$

Equation (2.21) is shown plotted in Figure (2.6) where fractional volume is plotted against resultant dielectric constant for the case of Perspex base dielectric (measured $K_1 = 2.60$). This graph will be used in the design of the lens in Chapter III.

2.3. RADIATION PATTERN CALCULATIONS

According to the geometrical optics developed in section (2.1), the Luneberg lens should have a parallel-sided radiated beam. Geometrical optics developments, however, do not include the effects of aperture diffraction. Since one wavelength of the radiated field is an appreciable fraction of the lens dimensions, divergence of the radiated beam will result. Calculation of the diffraction pattern involves an analysis similar to that used for optical

Fig. 2.6 - Dielectric constant as a function of fractional volume for Perspex.

$K_1 = 2.60$
$C = -0.258$

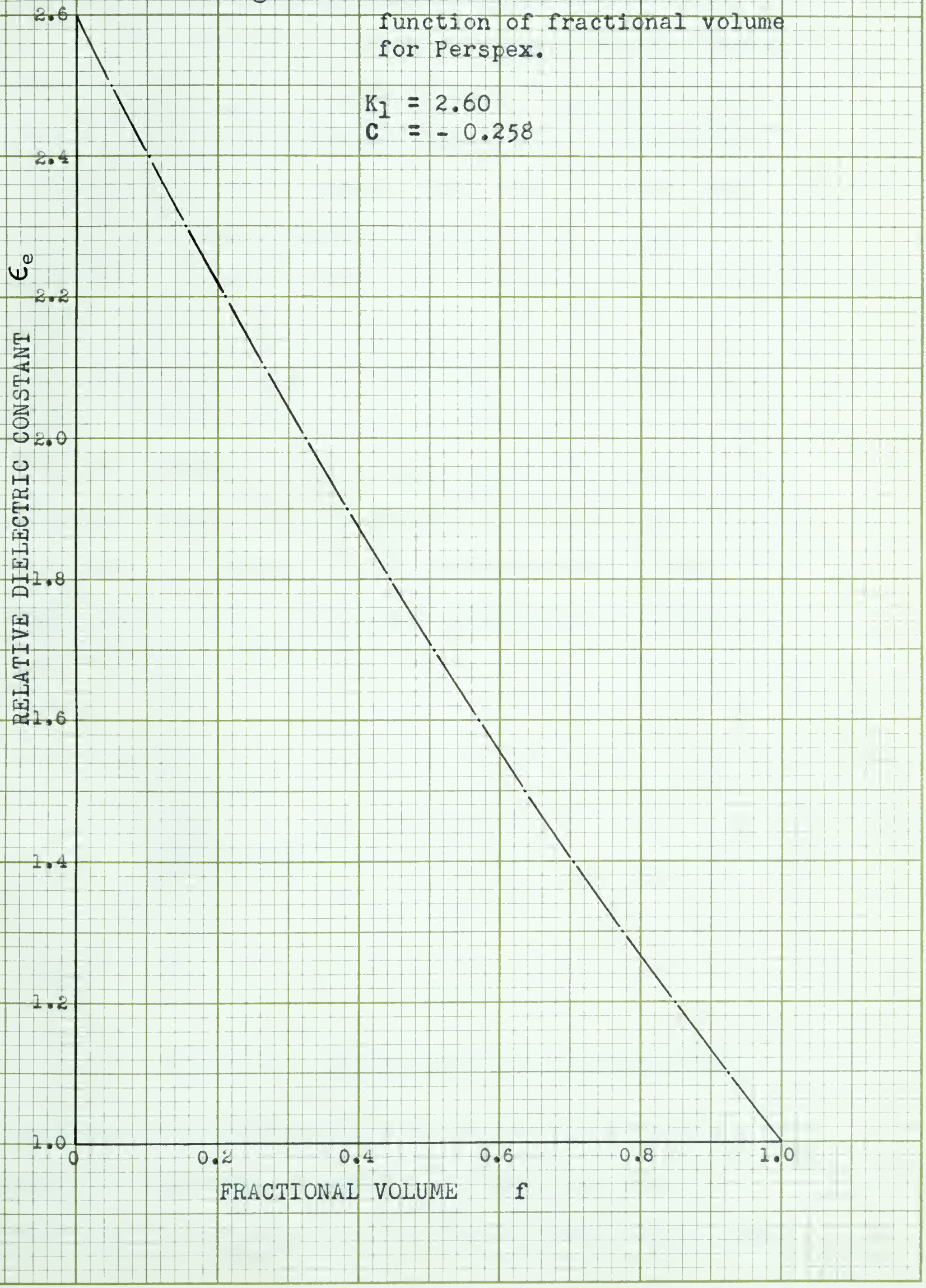

diffraction from a small circular aperture.

The diffraction field may be divided into three regions, each region boundary being determined by the nature of the approximations made in the mathematical formulation for that region. The first, the near-zone region, is in the immediate vicinity of the lens aperture. No approximations can be made in the diffraction field equation for this region. Beyond the near-zone lies the Fresnel region characterized by shadow zones and a rapidly changing pattern shape with increased distance from the aperture. Further still lies the Fraunhofer or far-zone region. The diffraction pattern in this region is usually of interest in microwave and radar lens applications where long-range propagation is required. The Fraunhofer diffraction pattern will be developed here.

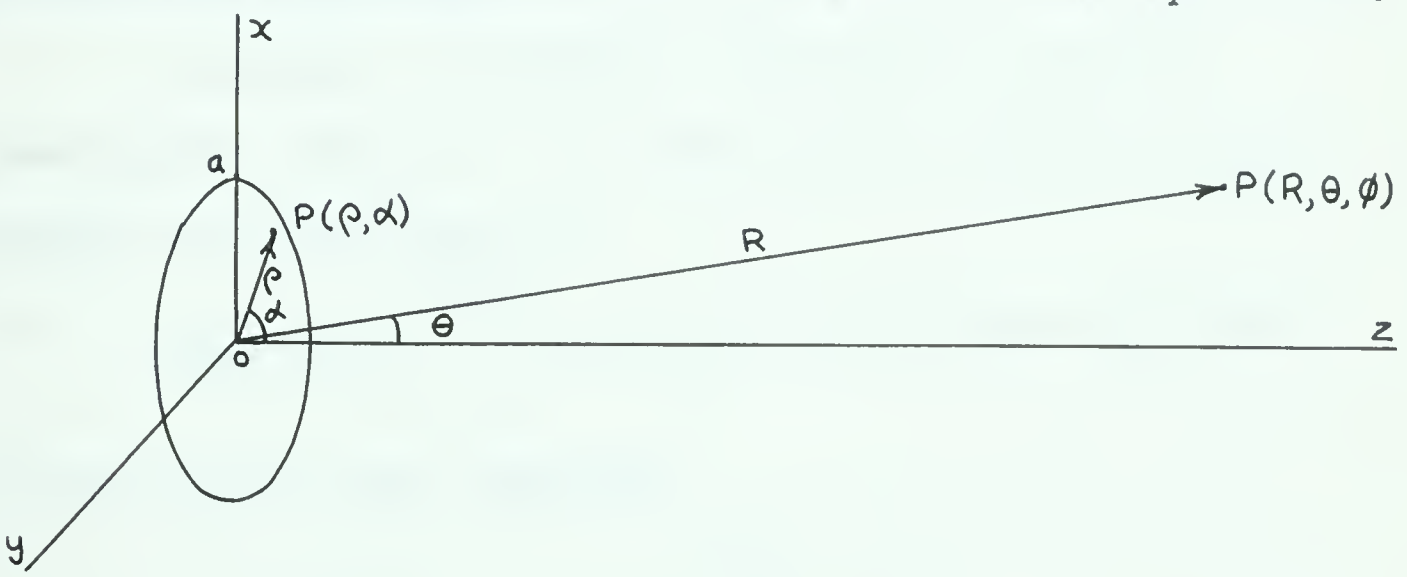

Fig. 2.7 - Diffraction field coordinates.

Consider a circular aperture of radius 'a' encircling the origin of a spherical coordinate system, as shown in Figure (2.7). Points on the aperture plane are defined

by polar coordinates ρ and α , while points in the diffraction field are defined by spherical coordinates R, θ and ϕ.

In the Fraunhofer region where $R >> a$, the radiation pattern is given by[23]

$$U_p = \frac{j}{\lambda R} \exp(-j\beta R) \int_0^{2\pi} \int_0^a F(\rho,\alpha) \exp\left[j\beta\rho \sin\theta \cos(\phi-\alpha)\right] \rho \, d\rho \, d\alpha \qquad (2.24)$$

where U_p is the electric field strength at point $P(R,\theta,\phi)$,

$F(\rho,\alpha)$ is the electric field strength distribution in the plane of the aperture,

β is the free-space propagation constant and

λ is the free-space wavelength.

Since electric field strength measurements are usually only relative, the amplitude term outside the integral need not be considered.

Consider a uniformly distributed aperture illumination, $F(\rho,\alpha) = 1$. The relative electric field strength is then given by

$$g(\theta,\phi) = \int_0^{2\pi} \int_0^a \exp\left[j\beta\rho \sin\theta \cos(\phi-\alpha)\right] \rho \, d\rho \, d\alpha$$

Introducing the new variables

$$r = \rho/a \quad , \quad u = \frac{2\pi a}{\lambda} \sin\theta$$

simplifies this equation to

$$g(u,\phi) = \int_0^{2\pi} \int_0^1 \exp\left[jur\cos(\phi-\alpha)\right] r \, dr \, d\alpha \qquad (2.25)$$

The pattern in the xz plane will be identical to the pattern in the yz plane because of circular symmetry. It is sufficient, therefore, to consider only one case, say the xz plane where $\phi = 0$. Integration over α gives

$$g(u) = \int_0^1 2\pi a^2 r J_0(ur)\, dr$$

and integration over r gives

$$g(u) = 2\pi a^2 \frac{J_1(u)}{u} \qquad (2.26)$$

where J_0 and J_1 are the zero-order and first-order Bessel function, respectively.

The power radiation pattern is proportional to the square of the electric field pattern. Figure (2.8) shows the diffraction pattern plotted in decibels against angle, for a 10-inch circular aperture and a free-space wavelength of 3.3 cms. This graph has been normalized to a maximum of zero decibels at an angle of zero degrees.

From this graph the characteristics of a 10-inch Luneberg lens operating at a frequency of nearly 9,200 Mc/s, are found and given below:-

Half-power beam angle is 7.6°

First side lobe is 17.5 dbs down

Angular position of first minimum is 8.3°

Angular position of first side lobe is 12°

These theoretical values will be compared with the actual values resulting from the Luneberg lens tests.

Fig. 2.8 - Far-field diffraction pattern for a circular aperture.

Aperture diameter = 10 inches
Wavelength = 3.3 cms.

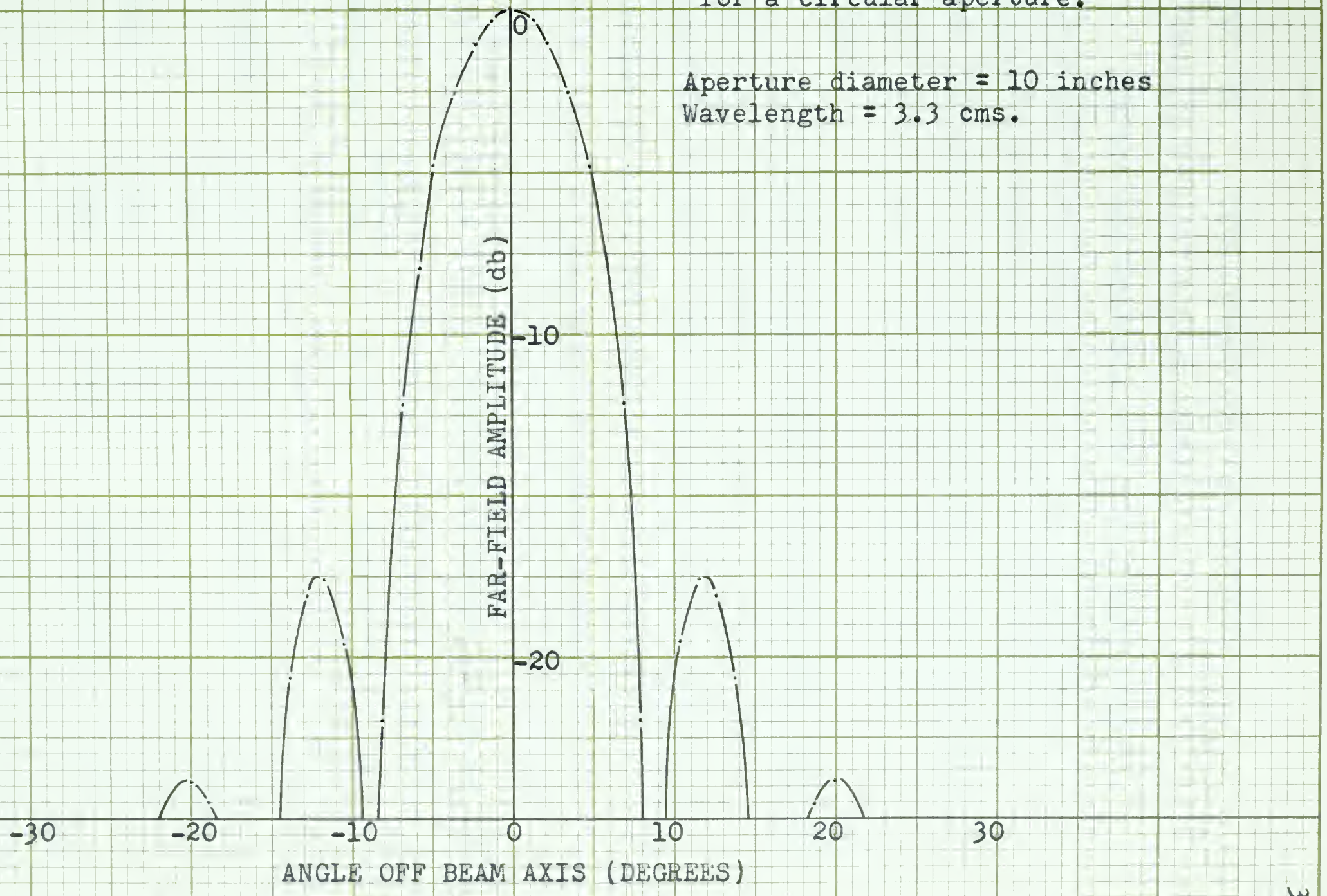

CHAPTER III LENS DESIGN AND CONSTRUCTION

3.1. VERIFICATION OF DESIGN EQUATIONS

Before the Luneberg lens was designed and constructed on the basis of the design equations developed in subsection (2.2.3), the equations were checked for their validity. Furthermore, the dielectric constant of the plastic material used (Perspex), had to be known.

As a check on the method of measurement, samples of two types of dielectrics, besides Perspex, were prepared and tested by the shorted-waveguide method of subsection (2.2.2). The results of these tests are shown in Table I along with published results.[24]

Table I. Solid Plastic Dielectric Constants at 9270 Mc/s

Material	Sample Length	Measured	Published	% Deviation
polystyrene	3 cm.	2.53	2.53-2.55	0
	5 cm.	2.50		-1.2
Plexiglas	5 cm.	2.58	2.59-2.60	-0.4
	6 cm.	2.56		-1.2
Perspex	5 cm.	2.61	none	----
	6 cm.	2.59	available	----

Both Perspex and Plexiglas are polymethyl methacrylates, the former is manufactured in England, the latter in the United States. Control conditions during manufacture probably account for any difference in the dielectric constants. The dielectric consfant of Perspex was taken

as 2.60.

The five centimeter sample of Perspex of the previous test was used to check the design equations (2.21), (2.22) and (2.23) as shown plotted in Figure (2.6). Cylindrical voids, of diameter approximately equal to their length, were machined into the sample and the dielectric constant was measured. The results of these measurements are shown in Table II together with the theoretical results obtained from the graph in Figure (2.6).

Table II. Dielectric Constants of Artificial Dielectric

K_1 = 2.60, Frequency = 9270 Mc/s, d = 5 cm.

Fractional Volume	Number of Voids	Measured	Calculated	% Error
0.020	1	2.57	2.56	-0.4
0.031	2	2.49	2.53	1.6
0.062	4	2.39	2.47	3.3
0.094	6	2.35	2.41	2.6
0.125	8	2.25	2.36	4.9
0.156	10	2.23	2.31	3.6
0.187	12	2.18	2.24	2.8
0.218	14	2.14	2.18	1.9
0.250	16	2.01	2.12	5.5
0.312	20	1.97	2.01	2.0

When the standing wave minimum occurs near the dielectric boundary, the accuracy of the measurements deteriorates because of the increased slope of the

dielectric constant curve for these readings (see Figure 2.5). The results of this measurement show that the calculated dielectric constant is, on the average, three percent higher than the measured value. The design equations can therefore be considered accurate to within about three percent.

3.2. LUNEBERG LENS DESIGN

The stepped-index, spherically symmetrical lens has been constructed by stacking 19 one-half inch Perspex discs, of different diameters, to form a 10-inch sphere. The refractive index was varied by adjusting the dielectric constant in each one-half inch annulus of each disc. Cylindrical voids, of appropriate diameter and number, were machined through each annulus. Calculations of the number and diameter of voids required were based on the equations of section (2.2.3), with two simplifications.

First, since the cylindrical void length is the same as the disc thickness, the fraction volume of equation (2.23) was modified to a fractional area concept where

$$f_A = \frac{N \pi D^2}{4A} \qquad (3.1)$$

Here D is the diameter of the void, N is the total number of voids per annulus and A is the annulus area. The void diameter is limited by the annulus width and by reflection considerations. The number of voids per annulus, is limited by the total number that can be fitted in the annulus while

still allowing for some mechanical strength. For this purpose, a strength factor was defined by

$$\text{strength factor} = \frac{\text{spacing between voids}}{\text{void diameter}} \qquad (3.2)$$

For larger values of void diameter, qualitative strength tests indicated that a strength factor of 1:10 was sufficient. For the small diameters, a strength factor of 1:5 was considered necessary.

The second simplification involves the Luneberg equation. Figure (3.1) shows a disc of radius b, located at a distance z from the center of the sphere.

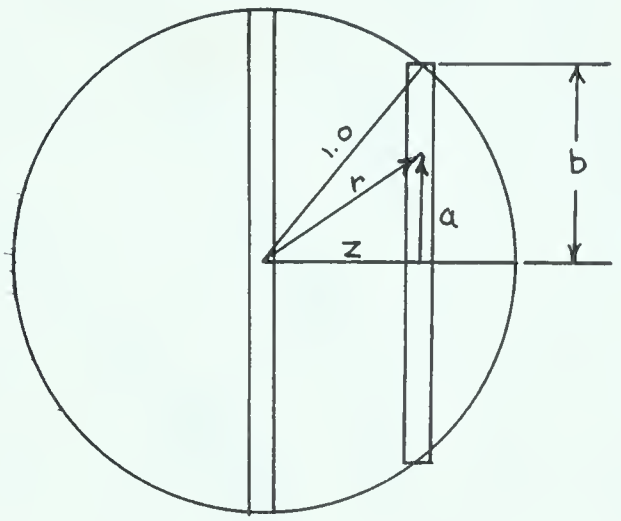

Fig. 3.1 - Stacked-disc Luneberg lens dimensions.

It is evident that the Luneberg equation can be written as

$$n^2 = \epsilon_e = 2 - r^2 = 2 - a^2 - z^2 \qquad (3.3)$$

Thus the required variation of the dielectric constant along any disc can be calculated from this equation. For convenience in design, this equation has been plotted for each of the ten discs. This graph is shown in Figure (3.2). In the actual design, each of these curves is approximated

Fig. 3.2 - Variation of dielectric constant along each disc as a function of normalized disc radius.

$$\epsilon_e = 2 - a^2 - z^2 = n^2$$

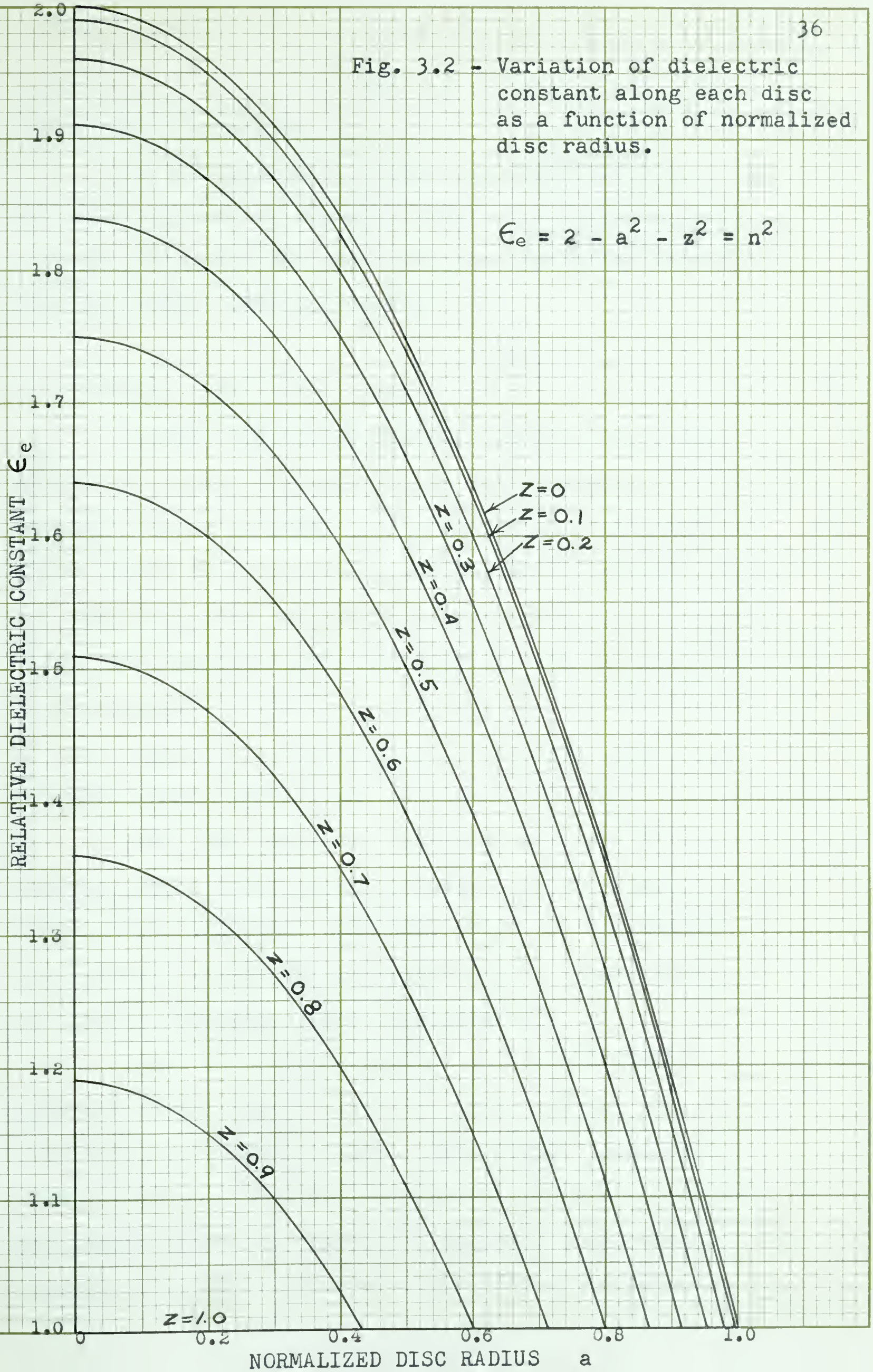

by one-half inch steps.

In the design, the discs are numbered from one to ten starting from the largest center disc and proceeding outward. The annuli for each disc are similarly numbered from the central annulus outward.

3.3. LUNEBERG LENS DESIGN TABLES

For any particular annulus, in any disc, the annulus area can be calculated. Also the average dielectric constant for that annulus can be found from the graph in Figure (3.2). With this value of dielectric constant known, the fractional area can be found from the graph in Figure (2.6). The required total void area can now be calculated. It then remains to choose a void diameter and the number of voids required, using equation (3.1), such that the strength factor requirements are also satisfied.

Table III gives the resultant design for the Luneberg lens. To aid in this design, use was made of Tables IV and V showing available drill cross-sectional areas and allowable annular drilled-out circumferences (to satisfy strength factor requirements).

Consider a sample design, say of the fifth annulus of disc number three. The total annulus area is found to be 7.08 square inches. From Figure (3.2) the average annulus dielectric constant is found to be 1.755. From Figure (2.6) the fractional area for a dielectric constant of 1.755 is found as 0.470. Since the annulus

area is 7.08 square inches, the total void area must be 7.08 X 0.47 = 3.33 square inches. If 30 voids are used, then the cross-sectional area of each void must be 3.33/30 = 0.111 square inches. From Table IV the obvious choice of void diameter is 3/8 inches since its cross-sectional area is just 0.111 square inches.

The strength factor requirement must also be satisfied. From Table V, for a strength factor of 1:10, the maximum allowable drilled-out circumference is 12.8 inches. 30 voids of 3/8 inch diameters amount to a drilled-out length of 30 X 0.375 = 11.2 inches. The strength factor requirement is therefore satisfied and annulus five of disc three will require 30 voids of 3/8 inch diameter.

For all the outer annuli, the fractional area requirements could not be satisfied since the required dielectric constant is near unity. To help satisfy this requirement, it was decided to make the outer one-quarter inch of each disc,air. This means that the actual Luneberg sphere is 9.5 inches in diameter but the effective sphere is 10 inches in diameter.

Table III. Void Radius and Void Number Determination.

Disc Number	Annulus Number	Dielectric Constant	Fractional Area	Void Area	Drill Diameter	Number of Voids
1	1	1.995	0.330	0.260	#6	8
	2	1.975	0.335	0.786	1/4	16
	3	1.935	0.360	1.42	9/32	22
	4	1.875	0.395	2.18	5/16	28
	5	1.795	0.445	3.15	23/64	32
	6	1.695	0.510	4.39	25/64	36
	7	1.575	0.582	5.94	27/64	42
	8	1.435	0.680	8.10	1/2	42
	9	1.275	0.792	10.60	7/16	54
	10	1.095	0.930	13.75	1/2	54
2	1	1.985	0.332	0.262	#5	8
	2	1.965	0.340	0.800	1/4	16
	3	1.925	0.363	1.43	19/64	21
	4	1.865	0.400	2.21	5/16	28
	5	1.785	0.450	3.19	3/8	30
	6	1.685	0.513	4.42	25/64	37
	7	1.565	0.590	6.02	27/64	43
	8	1.425	0.685	8.15	1/2	42
	9	1.265	0.800	10.72	7/16	54
	outer	1.090	0.930	12.95	1/2	54

Table III. Continued

Disc Number	Annulus Number	Dielectric Constant	Fractional Area	Void Area	Drill Diameter	Number of Voids
3	1	1.955	0.347	0.274	#4	8
	2	1.935	0.360	0.846	17/64	16
	3	1.895	0.385	1.52	5/16	20
	4	1.835	0.420	2.32	11/32	25
	5	1.755	0.470	3.33	3/8	30
	6	1.655	0.530	4.56	13/32	35
	7	1.535	0.612	6.24	7/16	41
	8	1.395	0.710	8.45	1/2	42
	9	1.235	0.820	11.0	7/16	55
	outer	1.075	0.942	11.0	25/64	60
4	1	1.905	0.380	0.300	#2	8
	2	1.885	0.390	0.916	17/64	16
	3	1.845	0.414	1.63	21/64	19
	4	1.785	0.450	2.48	23/64	25
	5	1.705	0.500	3.54	25/64	30
	6	1.605	0.565	4.86	27/64	35
	7	1.485	0.647	6.60	15/32	38
	8	1.345	0.740	8.80	1/2	42
	9	1.185	0.860	11.5	7/16	55

Table III. Continued

Disc Number	Annulus Number	Dielectric Constant	Fractional Area	Void Area	Drill Diameter	Number of Voids
5	1	1.835	0.420	0.332	#5	10
	2	1.815	0.430	1.01	9/32	16
	3	1.775	0.457	1.80	23/64	18
	4	1.715	0.495	2.73	3/8	25
	5	1.635	0.545	3.86	13/32	30
	6	1.535	0.610	5.26	7/16	35
	7	1.415	0.693	7.06	31/64	38
	8	1.275	0.792	9.40	1/2	42
	9	1.115	0.915	12.3	1/2	42
6	1	1.745	0.475	0.375	1/4	8
	2	1.725	0.490	1.15	19/64	16
	3	1.685	0.510	2.05	3/8	18
	4	1.625	0.550	3.03	25/64	25
	5	1.545	0.607	4.29	7/16	28
	6	1.445	0.670	5.78	15/32	33
	7	1.325	0.755	7.70	29/64	40
	8	1.185	0.860	10.2	1/2	42

Table III. Continued

Disc Number	Annulus Number	Dielectric Constant	Fractional Area	Void Area	Drill Diameter	Number of Voids
7	1	1.635	0.545	0.430	1/4	8
	2	1.615	0.560	1.32	21/64	16
	3	1.575	0.582	2.29	27/64	16
	4	1.515	0.625	3.45	15/32	20
	5	1.435	0.680	4.82	31/64	26
	6	1.335	0.747	6.44	29/64	34
	7	1.215	0.837	8.54	1/2	36
	8	1.075	0.942	11.2	7/16	48
8	1	1.505	0.630	0.497	1/4	10
	2	1.485	0.647	1.52	3/8	14
	3	1.445	0.670	2.64	15/32	15
	4	1.385	0.713	3.93	7/16	22
	5	1.305	0.770	5.45	31/64	26
	6	1.205	0.842	7.25	7/16	35
	7	1.085	0.935	9.54	1/2	36
9	1	1.355	0.735	0.58	1/4-3/8	8
	2	1.335	0.747	1.75	13/32	14
	3	1.295	0.780	3.07	7/16	16
	4	1.235	0.820	4.52	7/16	22
	5	1.155	0.882	6.24	7/16	29
	6	1.055	0.960	8.26	1/2	31

Table III. Continued

Disc Number	Annulus Number	Dielectric Constant	Fractional Area	Void Area	Drill Diameter	Number of Voids
10	1	1.185	0.860	0.68	1/4-3/8	12
	2	1.165	0.875	2.05	15/32	12
	3	1.125	0.905	3.57	7/16	16
	4	1.065	0.950	5.24	31/64	20

Dimensions: Annulus area in square inches

Void area in square inches

Drill diameter in inches or by drill index number

Drill cross-sectional area in square inches.

Table IV. Available Drill Cross-sectional Areas.

Drill Diameter	Drill Size	Cross-sectional Area	Drill Diameter	Drill Size	Cross-sectional Area
0.50	1/2	0.197	0.281	9/32	0.062
0.484	31/64	0.184	0.265	17/64	0.055
0.469	15/32	0.173	0.250	1/4	0.049
0.453	29/64	0.161			
0.437	7/16	0.150	0.288	#1	0.041
0.422	27/64	0.140	0.221	#2	0.038
0.406	13/32	0.129	0.213	#3	0.036
0.390	25/64	0.120	0.208	#4	0.034
0.375	3/8	0.111	0.205	#5	0.033
0.359	23/64	0.101	0.204	#6	0.0327
0.344	11/32	0.093	0.201	#7	0.032
0.328	21/64	0.084	0.199	#8	0.031
0.313	5/16	0.077	0.196	#9	0.030
0.297	19/64	0.069	0.193	#10	0.029

Table V. Allowable Annular Drilled-out Circumferences.

Annulus Number	Annulus Area	Mean Radius	Mean Circumference	Allowable Circumference SF = 1:10	SF = 1:5
1	0.79	0.25	1.57	1.11	0.95
2	2.35	0.75	6.29	5.66	5.03
3	3.94	1.25	7.86	7.07	6.28
4	5.52	1.75	11.0	9.90	8.80
5	7.08	2.25	14.2	12.8	11.4
6	8.62	2.75	17.3	15.6	13.9
7	10.2	3.25	20.4	18.4	16.4
8	11.9	3.75	23.6	21.2	18.8
9	13.4	4.25	26.8	24.1	21.3
10	14.8	4.75	29.9	26.9	23.9

SF is strength factor

3.4. CONSTRUCTION OF THE LENS

Machining of the voids was done with an electric drill-press. Like disc sizes were clamped together and machined at the same time. Considerable care had to be taken, during drilling, that inter-void cracking did not occur and that excessive heating did not cause melting of the plastic. Perspex reaches its softening point at a temperature of from 57 to 68 degrees Centigrade. The total number of voids machined in the sphere is in the neighborhood of 4400.

The individual discs were cut (after drilling was completed), with an electric-powered scroll-saw, at a

speed of 1200 rpm., using a steel blade. The discs in the sphere are held together by a number four plastic knitting needle.

Figure (3.3) shows the partly dissembled lens with the largest and the smallest discs shown in plane view. Several of the remaining discs are also shown in Figure (3.4) together with some of the dielectric samples used for the dielectric constant measurements. Figure (3.5) shows the completely assembled Luneberg lens, held together with the plastic knitting needle.

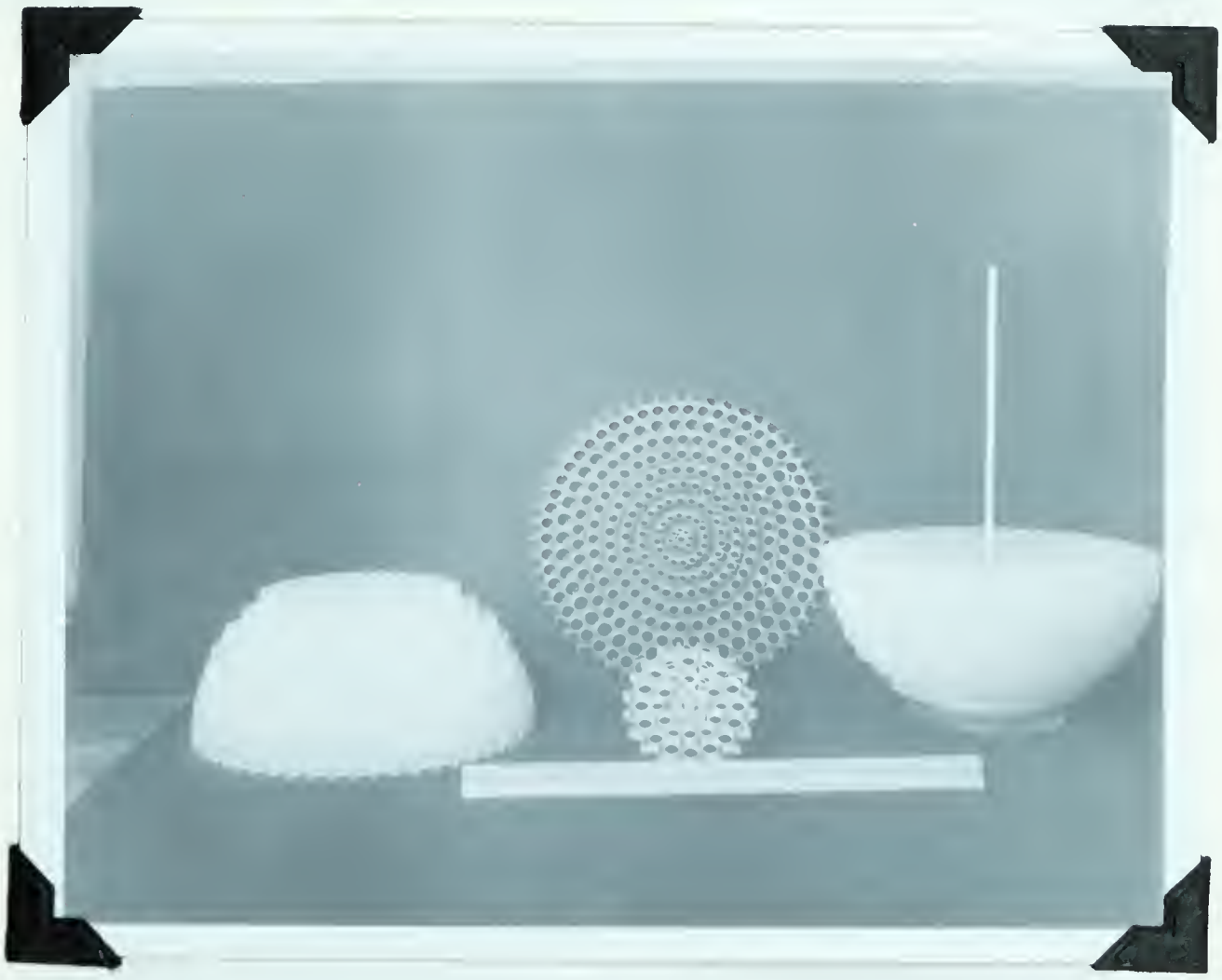

Fig. 3.3 - Partly dissembled stacked-disc Luneberg lens showing assembly method.

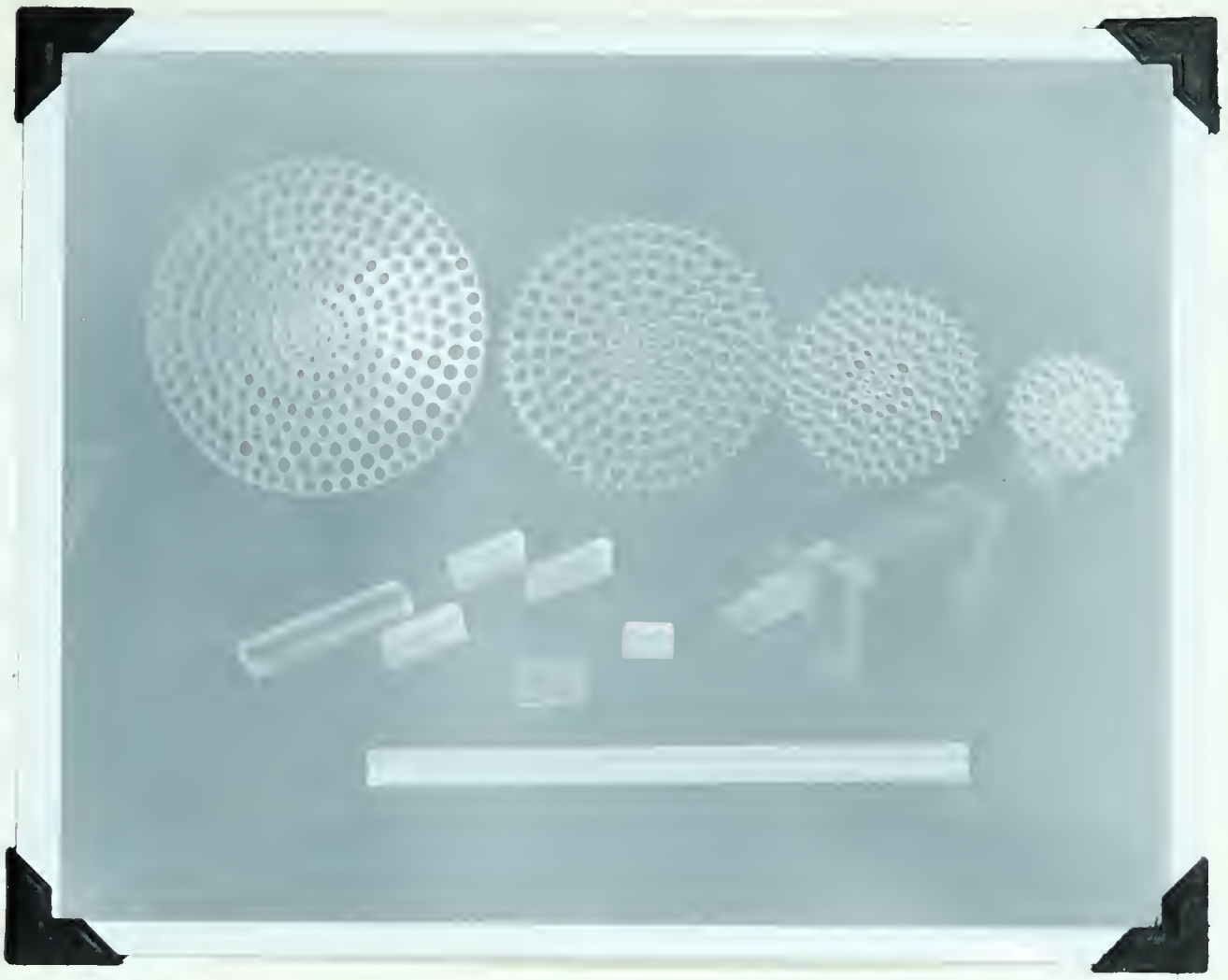

Fig. 3.4 - Luneberg lens discs and dielectric samples.

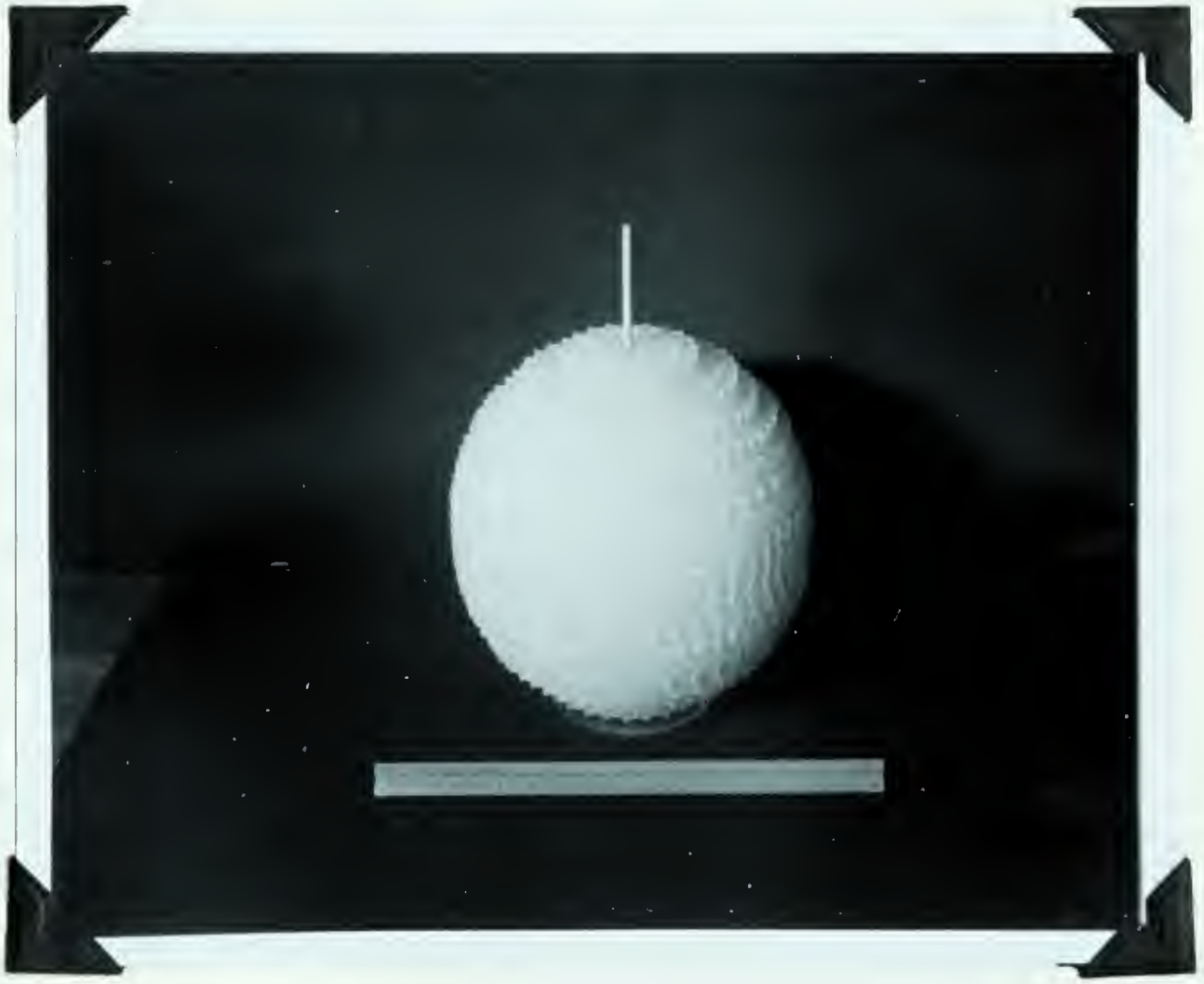

Fig. 3.5- The stacked-disc Luneberg lens.

CHAPTER IV MEASUREMENTS AND RESULTS

4.1. DESCRIPTION OF APPARATUS

A block diagram of the test setup for radiation pattern tests is shown in Appendix A. The component parts are described here.

The type 703 Polytechnic Research and Development X-band microwave generator, used for both dielectric constant and radiation pattern measurements, is shown in Figure (4.1). The generator consists of a type 723A/B reflex klystron feeding into an RG-52/U waveguide. The waveguide contains an uncalibrated attenuator and a cavity wavemeter operating in the TE_{10p} mode. This generator is shown connected to a Demornay Budd slotted waveguide and a 10-inch square aperture pyramid horn of slant height 25 inches. This equipment is designed to operate in the 8.4 to 9.6 KMc/s band with an average power output of 32 milliwatts.

The reflex klystron is powered by a Browning Labs. TVN-7 klystron power supply. Incorporated in the power supply is a variable frequency multivibrator with frequency range 600 to 2500 cps. Either the grid or the reflector of the klystron may be square-wave modulated. Figure (4.2) shows the power supply and the Hewlett-Packard 415A standing wave indicator. This indicator is a frequency-sensitive linear amplifier with a square-law calibrated scale. The indicator must therefore be used with a square-law detector, such as a crystal diode or a bolometer. The amplifier is sensitive to 1000 cps

which must be provided by amplitude modulating the RF voltage under measurement. Decibels and SWR may be read directly with this indicator or it may be used as a null detector.

Figure (4.3) shows the remote controlled servo-mechanism and the remote control indicator. The lens mounting and feed horn are also shown. The turning motor, controlled from the remote indicator position, rotates the lens mounting shaft. On this same shaft is coupled a synchro transmitter connected to a similar synchro receiver in the remote indicator. Onto the shaft of the receiver, is fixed a pointer which indicates the lens azimuthal angle. Rotation was allowed in one direction only because of slight amounts of backlash in the various couplings.

The feed horn is connected to a waveguide Tee. In the shorted arm of the Tee is a crystal diode. The output from this crystal is connected to the standing wave indicator, usually located at the remote control position. Thus rotation and measurements can be done from a remote position near the microwave generator.

4.2. LENS RADIATION PATTERNS AND CHARACTERISTICS

The Luneberg lens was subjected to six different sets of tests, each concerning itself with one aspect of the required and predicted lens characteristics. The first test checked that focusing ability of the lens. Patterns are shown for focused and defocused conditions. The second test investigated the effect of using different feed horns.

Fig. 4.1 - X-band microwave generator, slotted waveguide and pyramid horn.

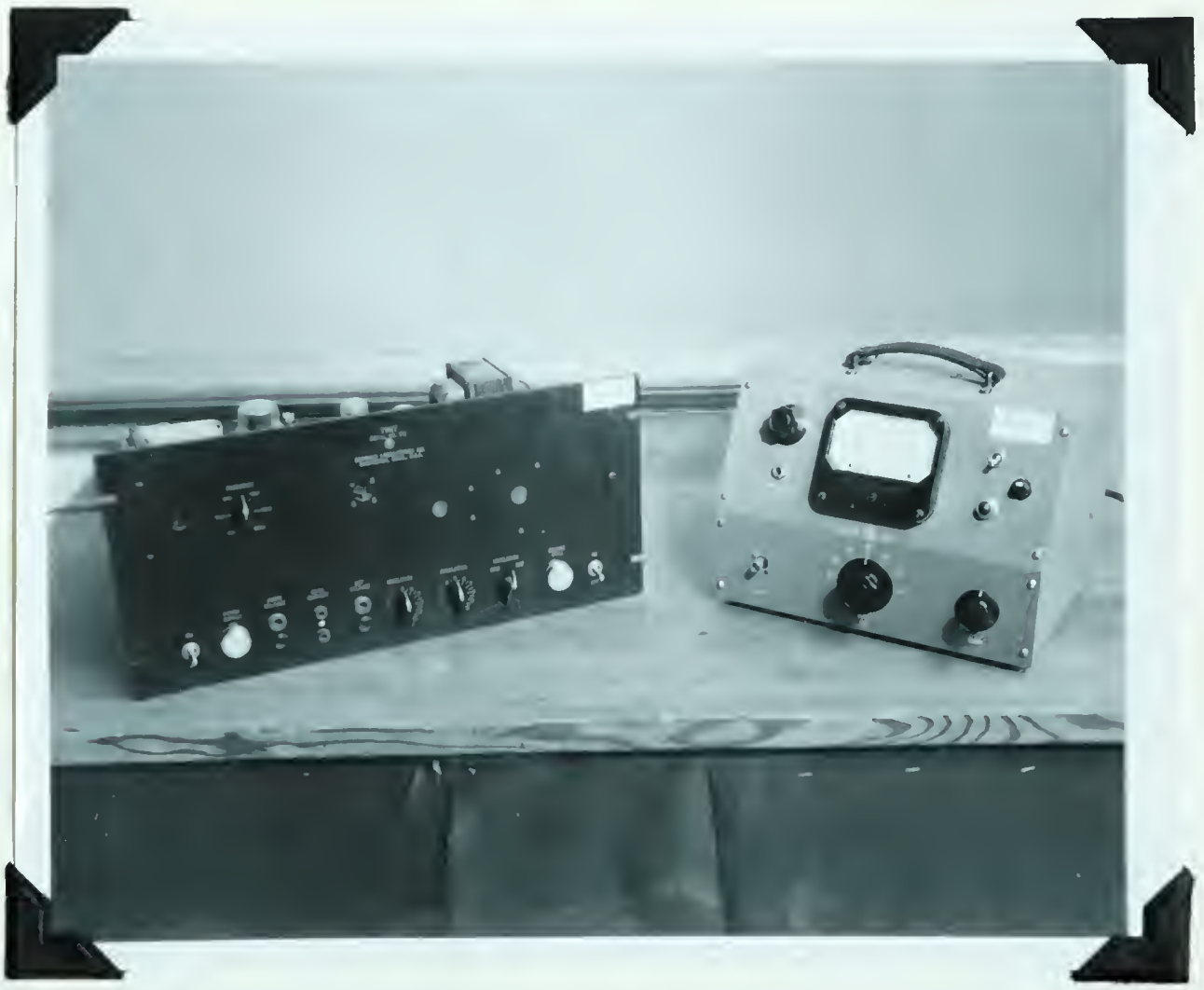

Fig. 4.2 - Klystron power supply and standing wave indicator.

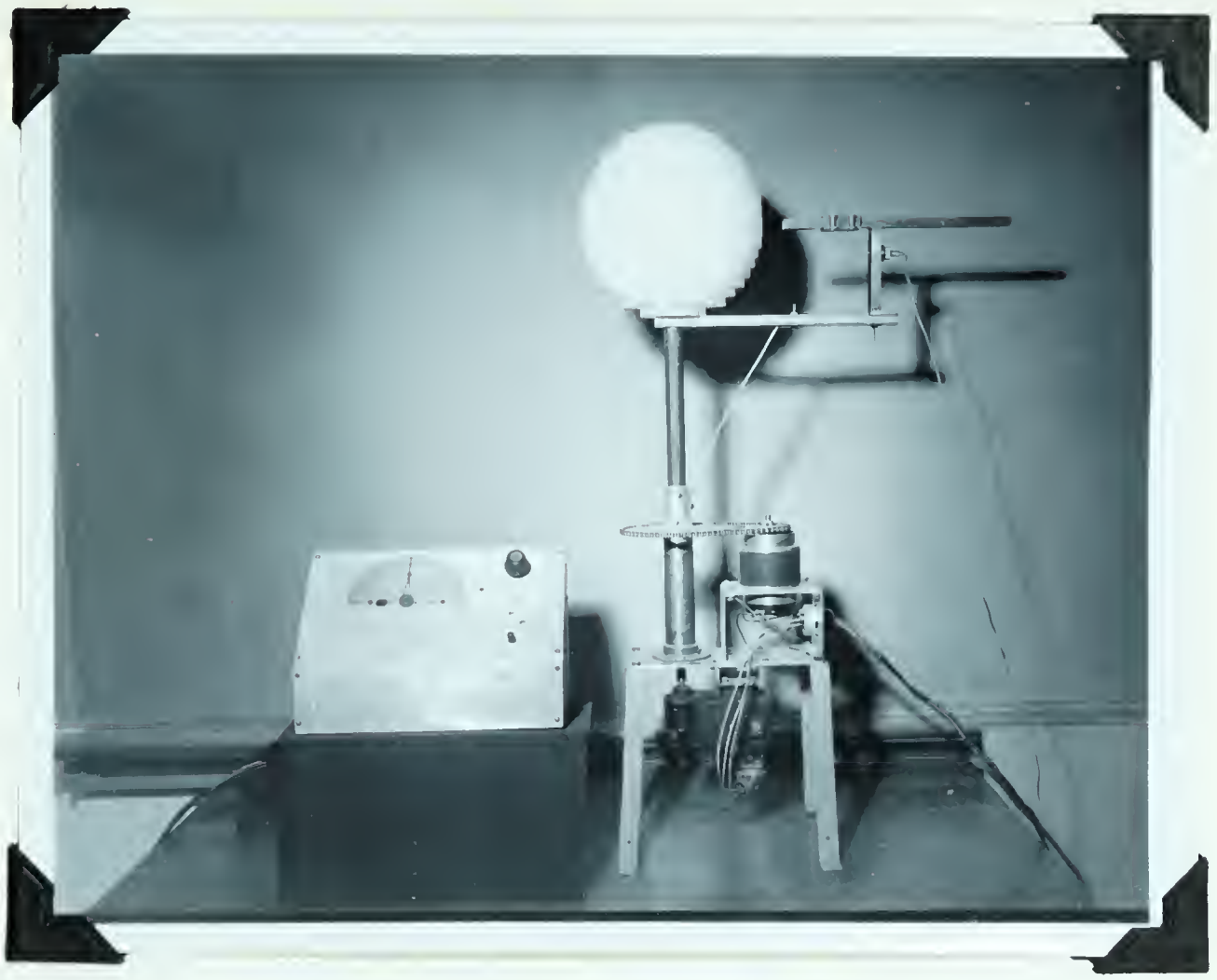

Fig. 4.3 - Remote control and indicator system showing the lens mounting and feed horn.

The third test attempted to determine the far-field distance and whether the lens was actually being tested in the far-field region. The fourth test investigated the operation of the lens at different frequencies, while the fifth test was a lens gain test.

For the sixth test, the optimum conditions were used, that is, the best conditions found from the previous five tests were set up and the lens was tested for symmetry and polarization.

For the five tests the lens was mounted as shown in Figure (4.3) but for a portion of the sixth test a special cup-shaped receptacle was fixed to the mounting shaft. The lens was then placed in this device on its side.

Three feed horns were used. They were, a sectoral horn, a waveguide horn and a waveguide horn-lens. The sectoral horn had an aperture width of 1 1/8 inches and a flare angle of 30^{o}. The waveguide horn was an open-ended waveguide and the waveguide horn-lens was an open-ended waveguide loaded with 5 centimeters of artificial dielectric of dielectric constant 2.00. The artificial dielectric was Perspex with cylindrical voids machined into it.

About 25 radiation patterns were recorded but several possessed too much similarity to be included. Only the most significant and the best patterns are shown.

1. Focus Test - The focusing ability of the lens was tested at a frequency of 9200 Mc/s and a source-lens separation of 12 feet. The E-field vector was perpendicular to the discs. Figure (4.4) shows radiation patterns for the sectoral horn at the focal point (horn aperture 3/4 inches from the lens surface) and for the feed horn in a defocused position of $1\frac{1}{2}$ inches from the lens surface. Shown also is a pattern where the feed horn was place against the lens surface.

Figure (4.5) shows a graph of field strength amplitude in decibels against feed horn displacement for the sectoral horn and the waveguide horn. The focal point of the former appears to be at 3/4 inches and the focal point of the latter is at 1/2 inches.

Figure (4.6) shows the variation in the field strength as the lens is rotated and the feed horn is kept in a fixed position. The sinusoidal-like variation has a period nearly equal to the spacing of the voids in the outer annuli of the center discs. The individual voids appear to be causing a lens-to-horn match as discussed by Morita and Cohn.[25]

2. Feed Horn Test - The effect of different feed horns on the radiation pattern is shown in Figure (4.7). Here the frequency was 9200 Mc/s, the distance was 12 feet and the E-field vector was perpendicular to the discs. The waveguide horn shows an improvement in the radiation pattern over the sectoral horn. For the waveguide horn, the side lobes are reduced, the minimums are more distinct, and the half-power beam angle is reduced by about one degree.

3. Distance Test - This test was carried out in effort to determine whether the radiation pattern tests were indeed being done in the far-zone region. For a 10-inch diameter lens, a distance of 12 feet would seem sufficient since then the separation would be considered large with respect to aperture diameter. It must be considered, however, that the pyramid horn is subject to diffraction effects too. A distance of 24 feet was chosen for a comparison test. Figure (4.8) shows that the improvement of the pattern with increased distance is almost insignificant. The beam angle remains constant while the side lobes are slightly reduced.

Fig. 4.4 - Focus test showing focused and defocused H-plane radiation patterns.

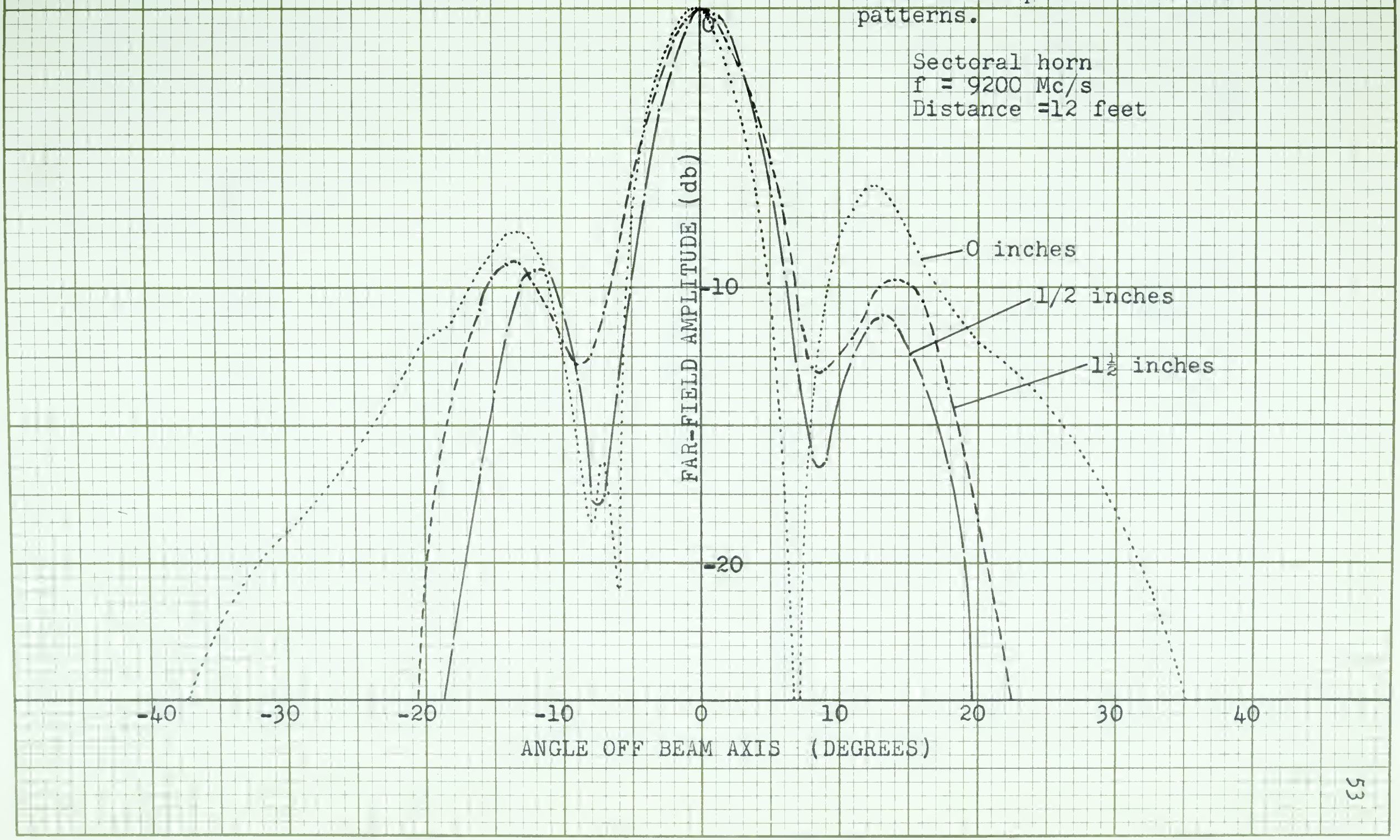

Fig. 4.5 - Focal point location

f = 9200 Mc/s
Distance = 12 feet
E-field ⊥r to discs

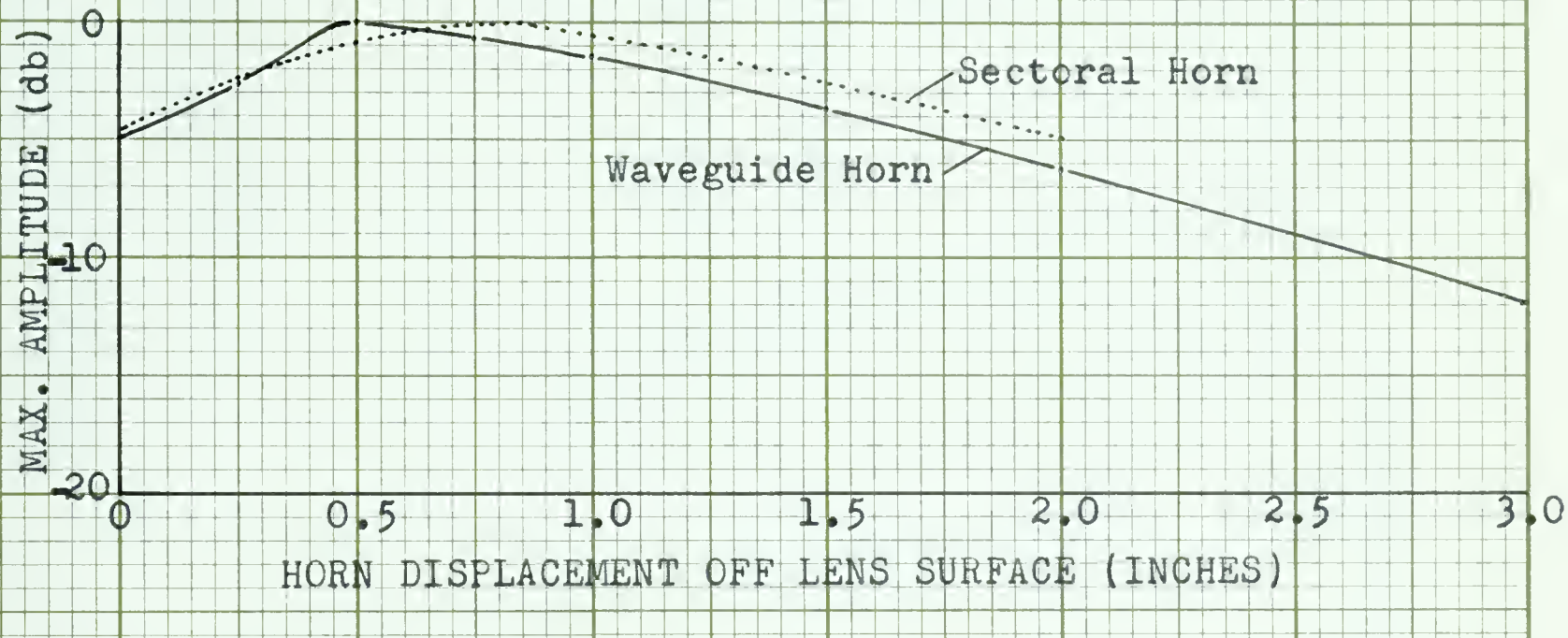

Figure 4.6 - Focal point variation with lens rotation.

f = 9200 Mc/s
Distance = 12 feet
E-field ⊥r to discs
Sectoral horn fixed

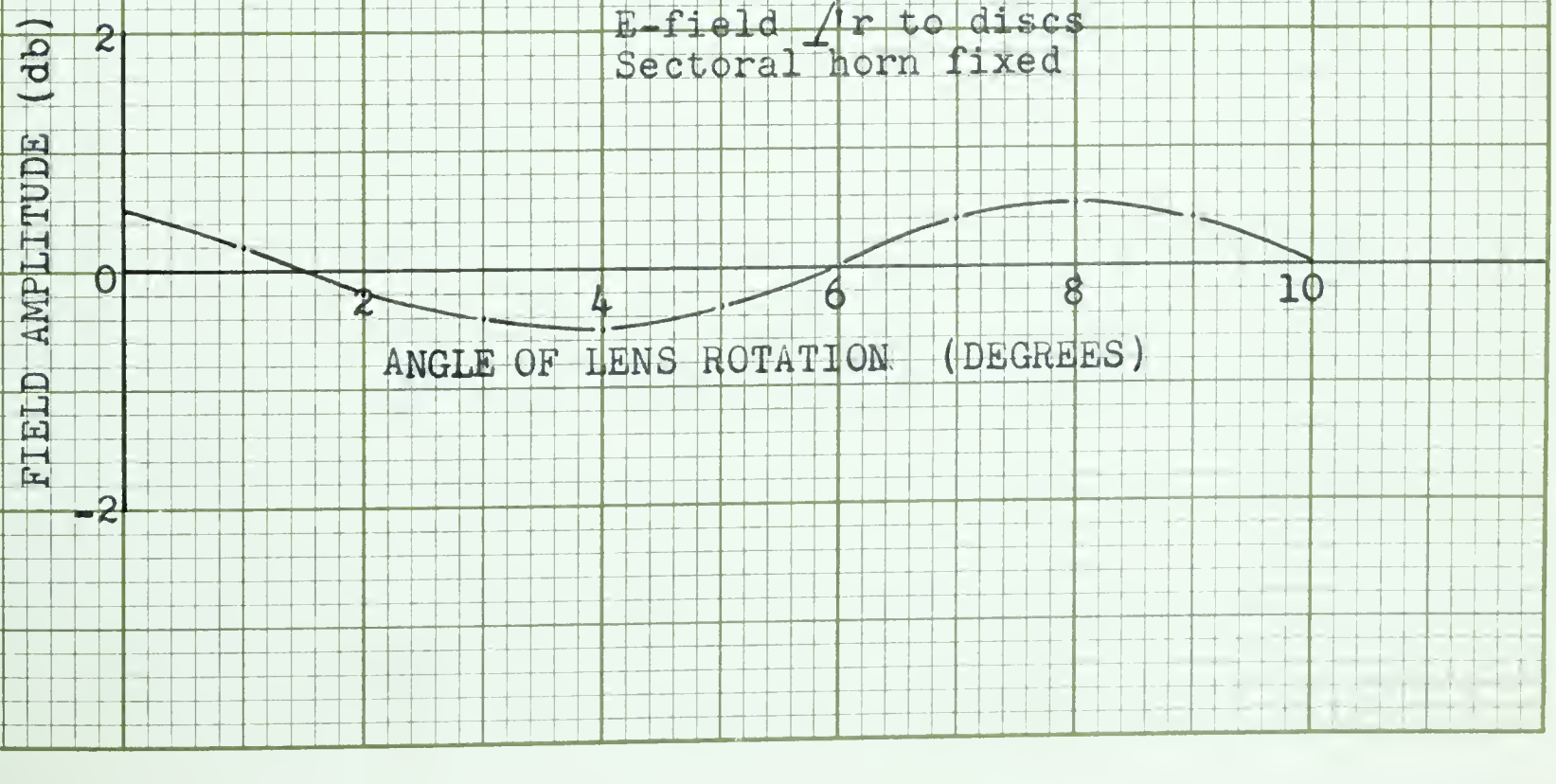

Fig. 4.7 - H-plane radiation patterns for different feed horns.

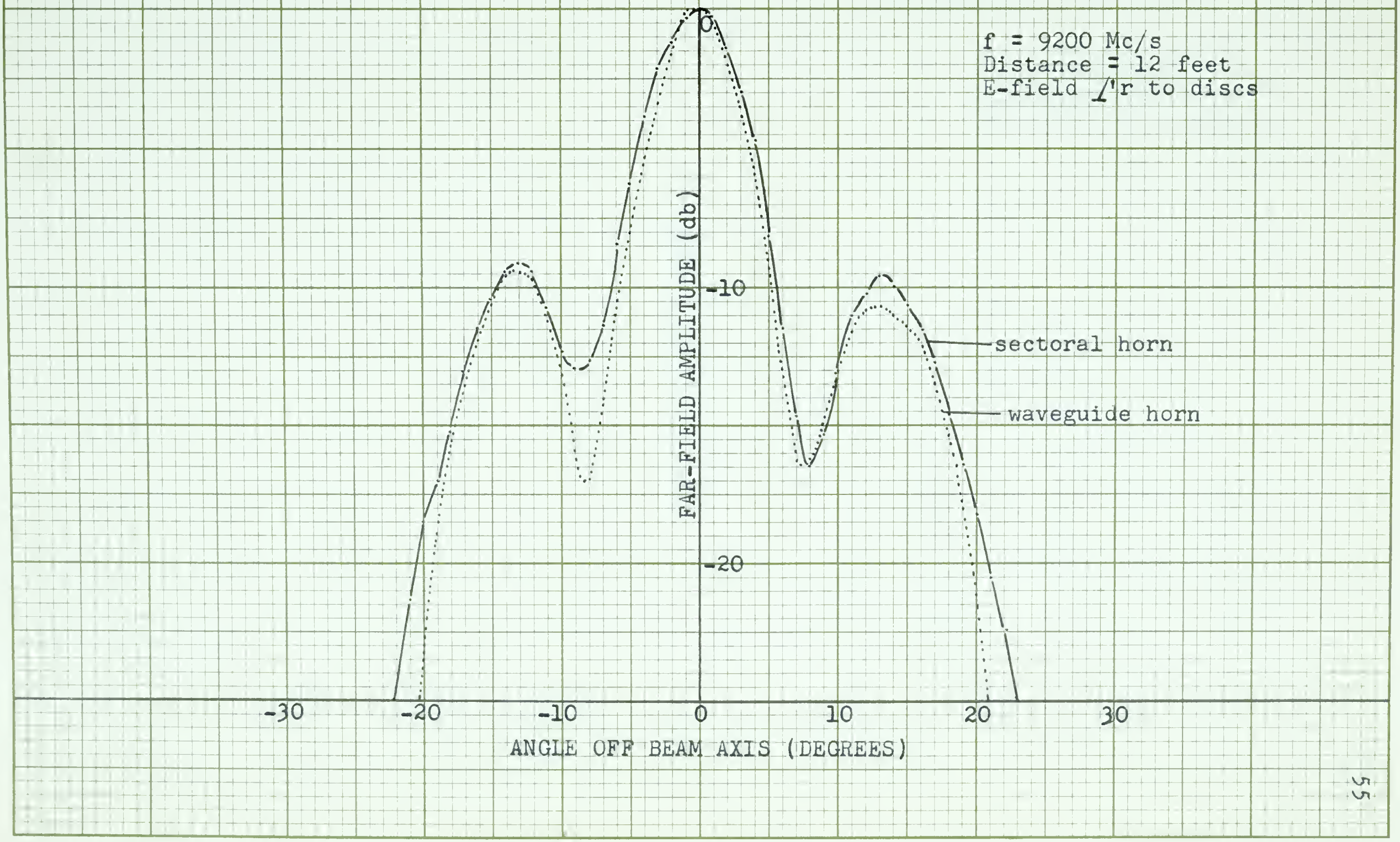

Fig. 4.8 - H-plane radiation patterns for different source-lens separations.

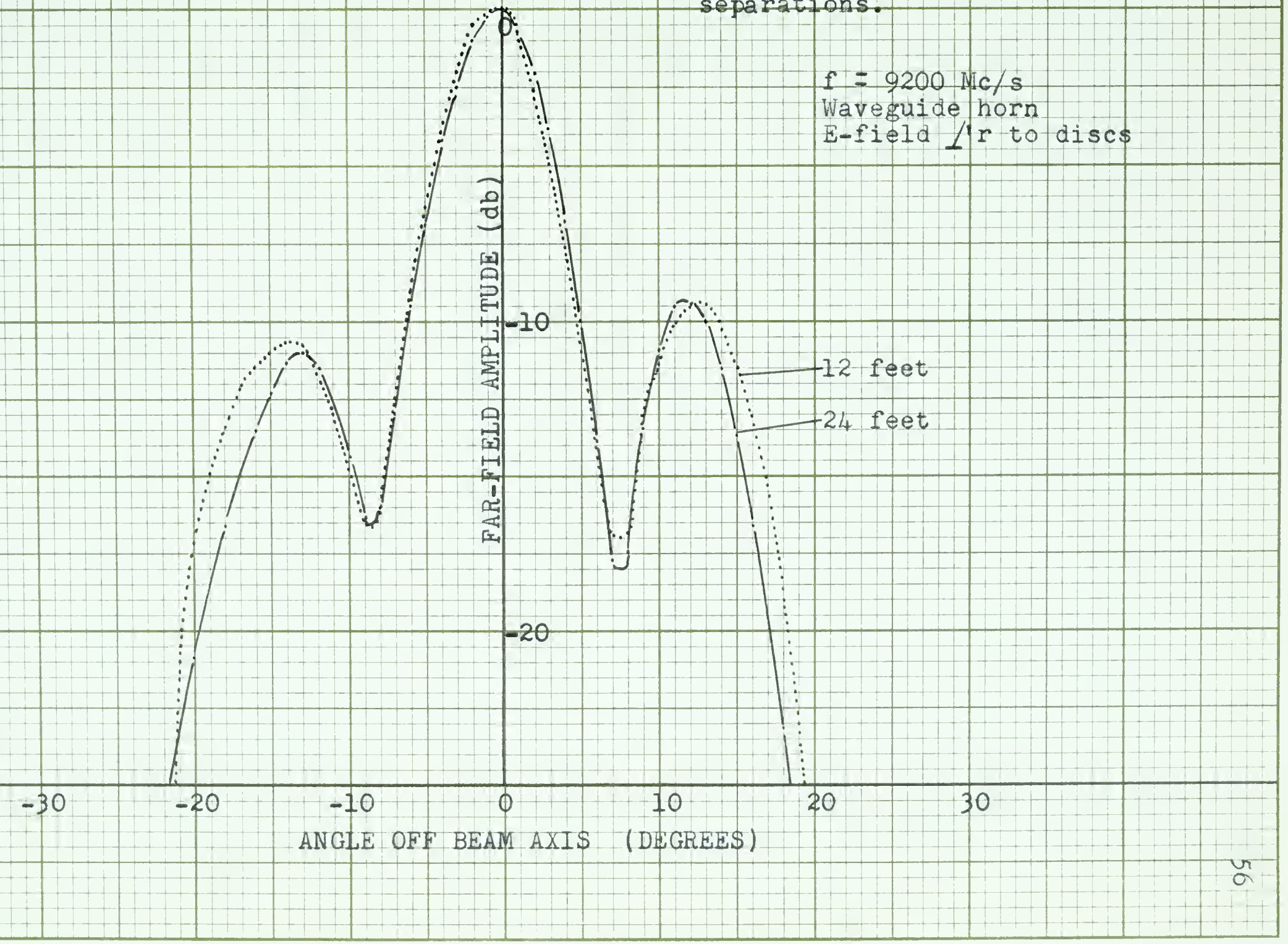

4. Frequency Test - Radiation patterns were recorded with a waveguide horn at a distance of 12 feet for frequencies of 8400 and 9200 Mc/s. The E-field vector was perpendicular to the discs. As can be seen from Figure (4.9), a decrease in frequency has the effect of broadening the main beam and moving the side lobes away from the main beam. This increased divergence with increased wavelength could have been predicted from diffraction theory. The accompanying reduction of the side lobe level is, however, attributed to the fact that at longer wavelengths the index of refraction variation in the lens appears to be more continuous than at shorter wavelengths. The design requires smaller steps in the index of refraction variation and smaller void dimensions coupled with an increased number of voids per annulus.

5. Gain Test - The power gain of a lens is the ratio of the main beam power of the lens to the power of a point source radiation uniformly in all directions. The theoretical power gain of a 10-inch circular aperture can be calculated as 580 or 27.6 dbs at a frequency of 9200 Mc/s. The Luneberg lens gain over a sectoral horn of aperture width 1 1/8 inches and flare angle of 30^{o} was found to be 21 dbs or 120. Since the theoretical gain of this sectoral horn is about 4.2 or 6.2 dbs, the measured value of 21 dbs seems reasonable for the Luneberg lens. Dielectric losses in the lens would account for any reduction in lens gain.

Fig. 4.9 - H-plane radiation patterns for different frequencies.

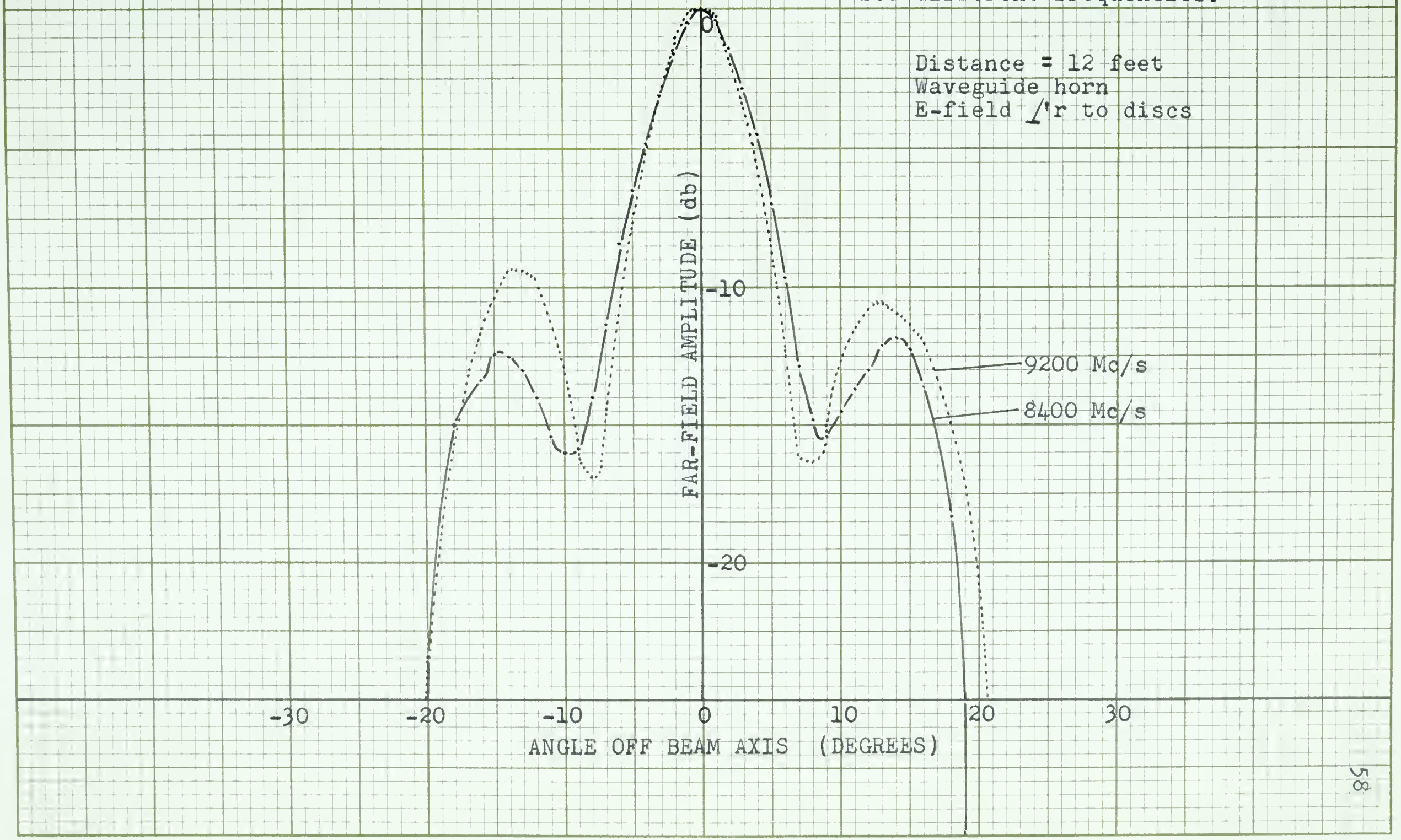

6. Optimum Conditions Test - The results of the previous five tests were used to set up an optimum conditions test. The frequency was set at 8400 Mc/s and the distance was set at 24 feet. In an effort to further improve the operation of the lens, a waveguide horn-lens was used as a feed horn. This feed horn consisted of an open-ended waveguide loaded with 5 centimeters of artificial dielectric, as described earlier. Figure (4.10) shows radiation patterns for the cases of the E-field vector perpendicular to the discs, and the E-field vector and the direction of propagation both parallel to the discs. It appears that the lens operates better in the former mode. The results of this part of this test indicate that the refractive index of the artificial dielectric is polarization-sensitive. Figure (4.11) shows the results of tests with the E-field vector and the direction of propagation both at 45^{o} to the discs and also with the E-field vector parallel to the discs while the direction of propagation was perpendicular to the discs (propagation along the axes of the voids). Again the lens appears to be somewhat nonisotropic.

Figure (4.12) shows a polar plot of the pattern of Figure (4.11) where both the E-field vector and the direction of propagation were at 45^{o} to the discs. This pattern is plotted using relative field strength rather than decibels.

Fig. 4.10 - H-plane radiation patterns showing the effects of polarization changes.

f = 8400 Mc/s
Distance = 24 feet
Waveguide horn-lens

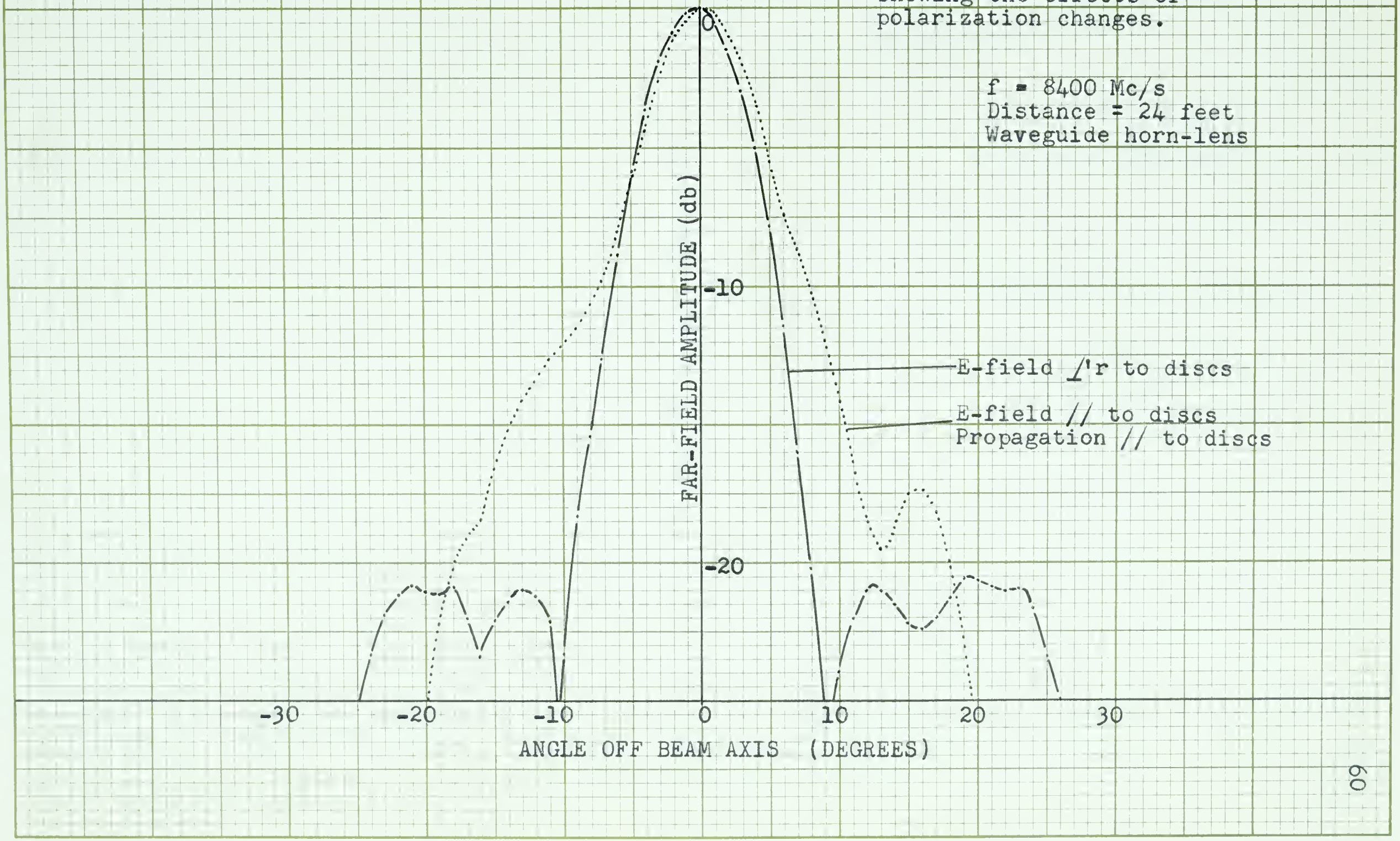

Fig. 4.11 - H-plane radiation patterns showing the effects of different propagation directions.

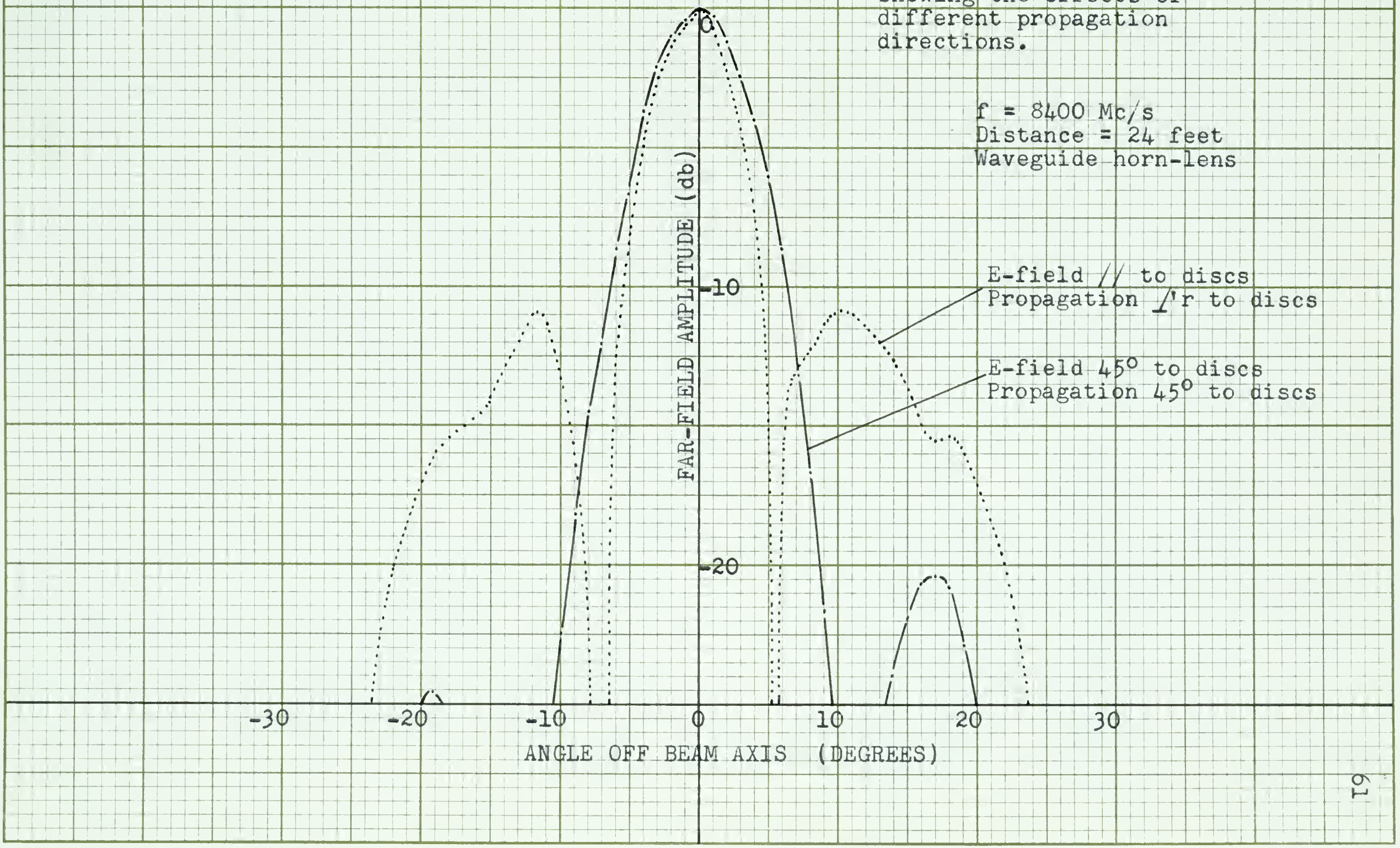

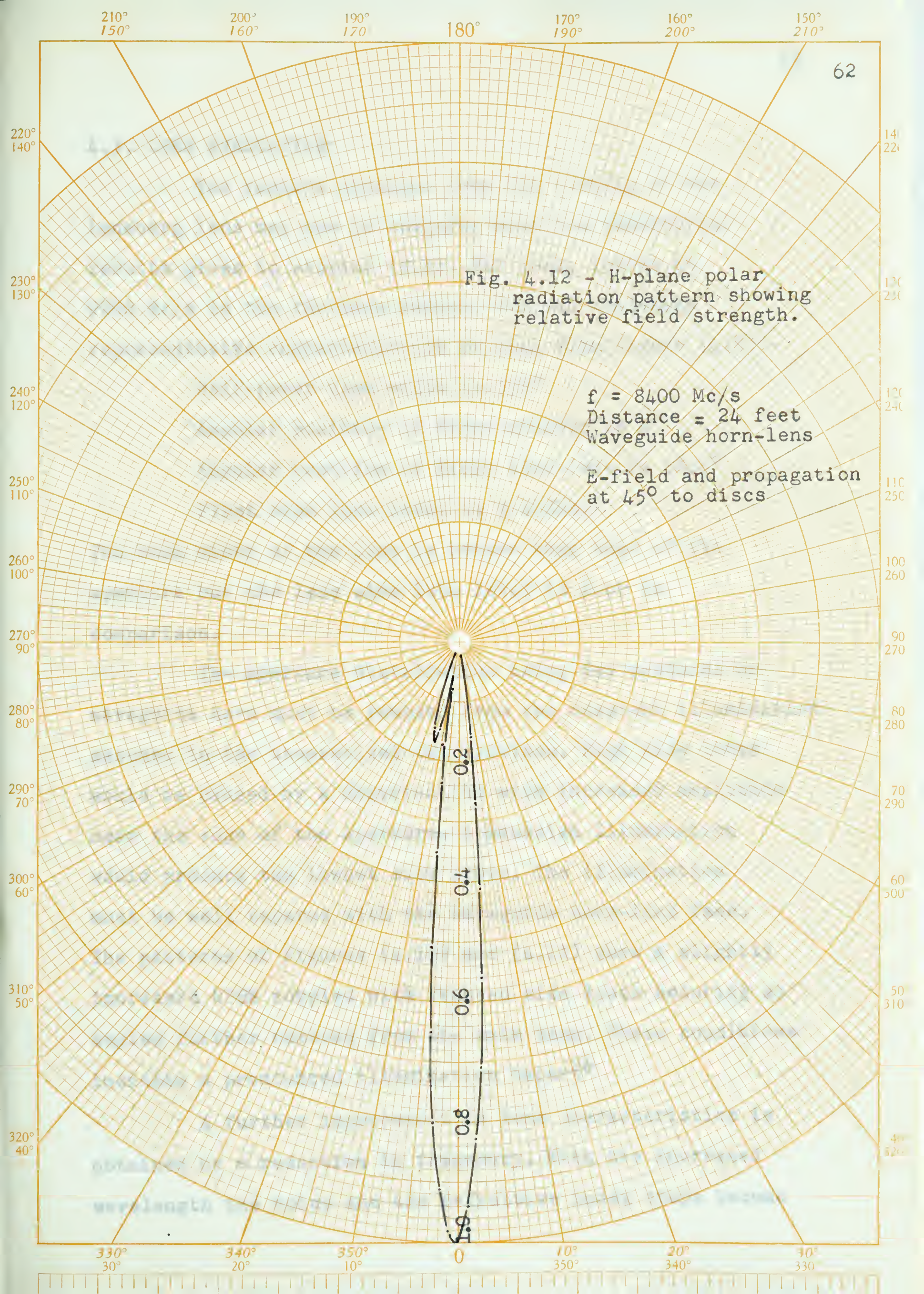

Fig. 4.12 - H-plane polar radiation pattern showing relative field strength.

f = 8400 Mc/s
Distance = 24 feet
Waveguide horn-lens

E-field and propagation at 45° to discs

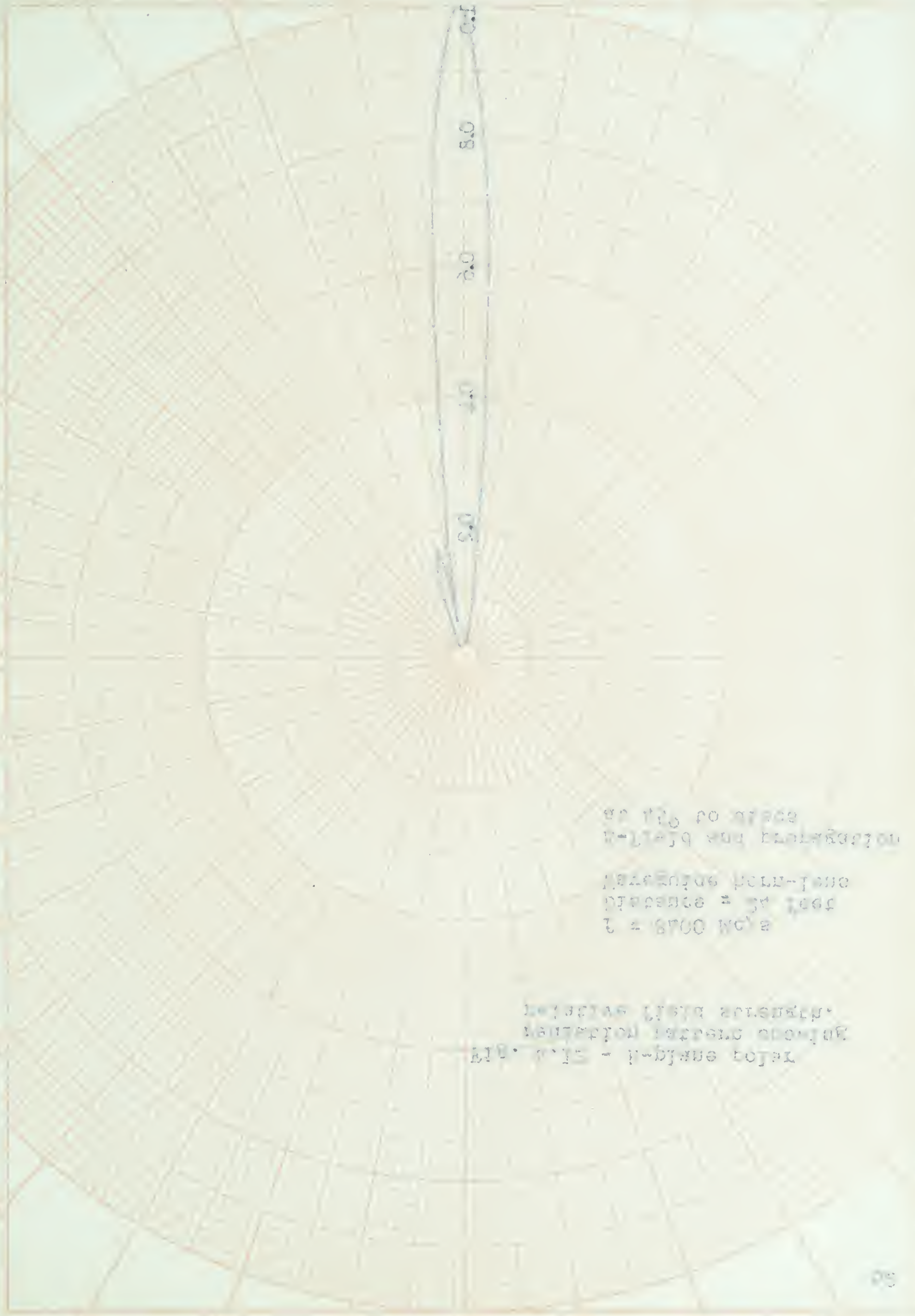
6.0
8.0
10
12
14

4.3. LENS EVALUATION

The results obtained from the testing of the Luneberg lens may now be compared with the theoretical results given in section (2.3). The lens, tested at 9200 Mc/s in the far-zone region, has the following representative characteristics as seen from Figure (4.8):-

Half-power beam width is 5.8^{o}

Angular position of first minimum is 8^{o}

Angular position of first side lobe is 12.5^{o}

First side lobe level is 9.4 dbs.

The beam width of the lens is better than that of the aperture but the lens side lobe level is poor in comparison.

The aperture distribution using the sectoral or waveguide horn must be removed from the constant illumination assumed in the theoretical calculations. High side lobes would be caused by a distribution with increased amplitude near the edge of the aperture. A Gaussian illumination would produce the lowest side lobes. The illumination must be well tapered with the waveguide horn-lens feed. The patterns of Figures (4.10) and (4.11) show a slightly increased HPBW coupled with reduced side lobes occuring at angles farther removed from the main beam. These conditions indicate a pronounced illumination taper.[26]

A further improvement in lens characteristics is obtained by a reduction in frequency. With the increased wavelength the voids and the refractive index steps become

relatively smaller causing less discontinuity and reduced reflections.

The characteristics of the Luneberg lens under the best conditions are, from Figure (4.10):-

Half-power beam width is 6.6°

Angular position of first minimum is 9.5°

Angular position of first side lobe is about 12.5°

First side lobe is 20.5 dbs down from peak.

The lens characteristics are poor when the E-field vector is perpendicular to axes of the voids and the direction of propagation is either perpendicular to the void axes or parallel to them. This does not discourage the use of the lens as a radar radiating device. Consider the lens mounted with the discs horizontal and the illumination vertically polarized. If the feed circle plane is horizontal, Figure (4.10) shows that the radiated beam has the desired shape. If the feed circle plane is tilted up to an angle of 45° or more, the lens still produces a very narrow beam with practically non-existent side lobes as shown in Figure (4.11) and (4.12). If the illumination is horizontally polarized or the zenith is being scanned, then the beam produced is degenerate. As a radar wide-angle scanning device, therefore, the Luneberg lens constructed has potential.

CHAPTER V CONCLUSIONS

5.1. ECONOMIC CONSIDERATIONS

Perspex is manufactured in England. In the United States the equivalent methacrylate is Plexiglas and in Canada, Canadian Industries, Ltd., manufactures this plastic under the trade name of Acrylic. Perspex can be imported into Canada at a cheaper price than Plexiglas. Prices for these plastics vary somewhat but at the time of purchase, the retail prices of these plastics were:-

Perspex ; 1/4 inch sheet, per square foot, $2.10
3/8 inch sheet, per square foot, $3.35
1/2 inch sheet, per square foot, $5.50
Plexiglas; 1/2 inch sheet, per square foot, $6.25
Acrylic; 1/2 inch sheet, per square foot, $5.75

Since Perspex is sold in square sheets, a certain amount of wastage is expected in manufacturing a spherical lens. For a 10-inch lens, about 12 square feet of 1/2 inch sheet must be purchased at a cost of about $62.00.

Other plastic materials such as polyethhylene, polystyrene, Teflon, Lucite, Styrofoam and Bakelite are more expensive or more difficult to obtain.

5.2. DISCUSSION

It is considered that this investigation has shown that a Luneberg lens with good characteristics, can be constructed from flat plastic discs by cutting the discs to the appropriate diameters and stacking them to form a spherical shape. Further it has also been shown

that the index of refraction in the Luneberg lens can be varied by perturbing the base dielectric.

The operation of the lens is dependent on the aperture illumination and the frequency. Several improvements in the design can be suggested now. The void dimensions should be reduced if higher frequencies are contemplated. The index of refraction should also be varied in smaller steps, say one-quarter inch steps. This would require the use of thinner Perspex sheets. A base dielectric of lower dielectric constant would require fewer or smaller voids to give the same dielectric constant variation. A material such as Teflon with a dielectric constant of 2.02 would be ideal since the dielectric constant required at the center of the lens is 2.00. The outer discs could also be formed from a dielectric with a constant nearer to unity.

Further improvements in the feed horn can be attempted using suggestions outlined by Webster.[27] A short-focus horn[7] could be attempted. The short-focus horn, which gives a near Gaussian distribution, could be manufactured from perturbed plastic material also.

The Luneberg lens constructed and tested is considered as a successful lens for radar and microwave applications. The design, construction and testing was found to be very interesting and instructive.

BIBLIOGRAPHY

1. Kock, W.E.,"Metallic delay lenses", Bell Sys. Tech. Jour., vol. 27, pp. 77-80; January, 1948.
2. Kay, A.F.,"Spherically symmetric lenses", Trans. IRE, vol. AP-7, no.1, pp. 32-38; January, 1959.
3. Goatley, C. and Parker, C.F.,"Symmetrical microwave lenses", IRE Convention Record, vol. 3, pt. I, pp. 13-19; 1955.
4. Kelleher,K.S. and Goatley, C.,"Dielectric lens for microwaves", Electronics, vol. 28, pp. 142-145; August, 1955.
5. Kelleher, K.S.,"Designing dielectric microwave lenses," Electronics, vol. 29, pp. 138-142; June, 1956.
6. Morrow, C.W., Taylor, P.E. and Ward, H.T.,"Phase and amplitude measurements in the near field of microwave lenses", IRE Convention Record, vol. 6, pt. I, pp. 166-176; 1958.
7. Brown, J.,"Microwave Lenses", Metheun & Co., Ltd., London, England, 1953.
8. Luneberg, R.K.,"Mathematical Theory of Optics", Brown University Press, Providence, R.I., pp. 208-213; 1944.
9. Brown, J.,"Microwave wide-angle scanner", Wireless Eng., vol. 30, pp. 250-255; October, 1953.
10. Gutman, A.S.,"Modified Luneberg lens", Jour. Appl. Phys., vol. 25, pp. 855-859; July, 1954.
11. Morgan, S.P.,"General solution of the Luneberg lens problem", Jour. Appl. Phys., vol. 29, pp. 1358-1368; September, 1958.
12. Kay, A.F.,"The impossibility of certain Luneberg lens modifications", Trans. IRE, vol. AP-4, pp. 87; January, 1956.

13. Huynen, J.R.,"Theory and design of a class of Luneberg lenses", IRE Convention Record, vol. 2, pt. I, pp.219-230; 1958.

14. Peeler, G.D.M. and Coleman, H.P.,"Microwave stepped-index Luneberg lens", Trans. IRE, vol. AP-6, no.2, pp. 202-207; April, 1958.

15. Sarbacher, R.I. and Edson, W.A.,"Hyper and Ultrahigh Frequency Engineering", John Wiley & Sons, Inc., New York, 1944.

16. Saito, S. and Kurokawa, K.,"A precision resonance method for measuring dielectric constant of low-loss solid materials in the microwave region", Proc. IRE, vol. 44, no. 1, pp.35; January, 1956.

17. Roberts, S. and von Hippel, A.,"Dielectrics in Waveguides", Jour. Appl. Phys., vol. 17, pp. 610; July, 1946.

18. Dakin, T.W. and Works, C.N.,"Microwave dielectric measurements", Jour. Appl. Phys., vol. 18, pp. 789; September, 1947.

19. Bowie, D.M. and Kelleher, K.S.,"Rapid measurement of dielectric constant and loss tangent", Trans. IRE, vol. MTT-4, no.3, pp. 137-140; July 1956.

20. Corkum, R.W.,"Isotropic artificial dielectric", Proc. IRE, vol. 40, no. 5, pp. 574-587; May, 1952.

21. Ward, H.T., Puro, W.O. and Bowie, D.M.," Artificial Dielectric utilizing cylindrical and spherical voids", Proc. IRE, vol. 44, no. 2, pp. 171-174; February, 1956.

22. Bottcher, C.J.F.,"Theory of Electrical Polarization", Elsevier Publishing Co., New York, pp. 51,61; 1952.

23. Silver, N.,"Microwave Antenna Theory and Design", McGraw-Hill Book Co., Inc., New York, pp. 169; 1948.

24. Von Hippel, A.R.,"Dielectric Materials and Applications", John Wiley & Sons, Inc., New York, 1948.

25. Morita, T. and Cohn, S.B.,"Microwave lens matched by simulated quarter-wave transformers", Trans. IRE, vol. AP-4, no. 1, pp. 33; January, 1956.

26. Braun, E.H.,"Radiation characteristics of the spherical Luneberg lens", Trans. IRE, vol. AP-4, no. 2, pp. 132-138; April, 1956.

27. Webster, R.E.,"Radiation patterns of a spherical Luneberg lens with simple feeds",Trans. IRE, vol. AP-6, no. 3, pp. 301-302; July, 1958.

APPENDIX A

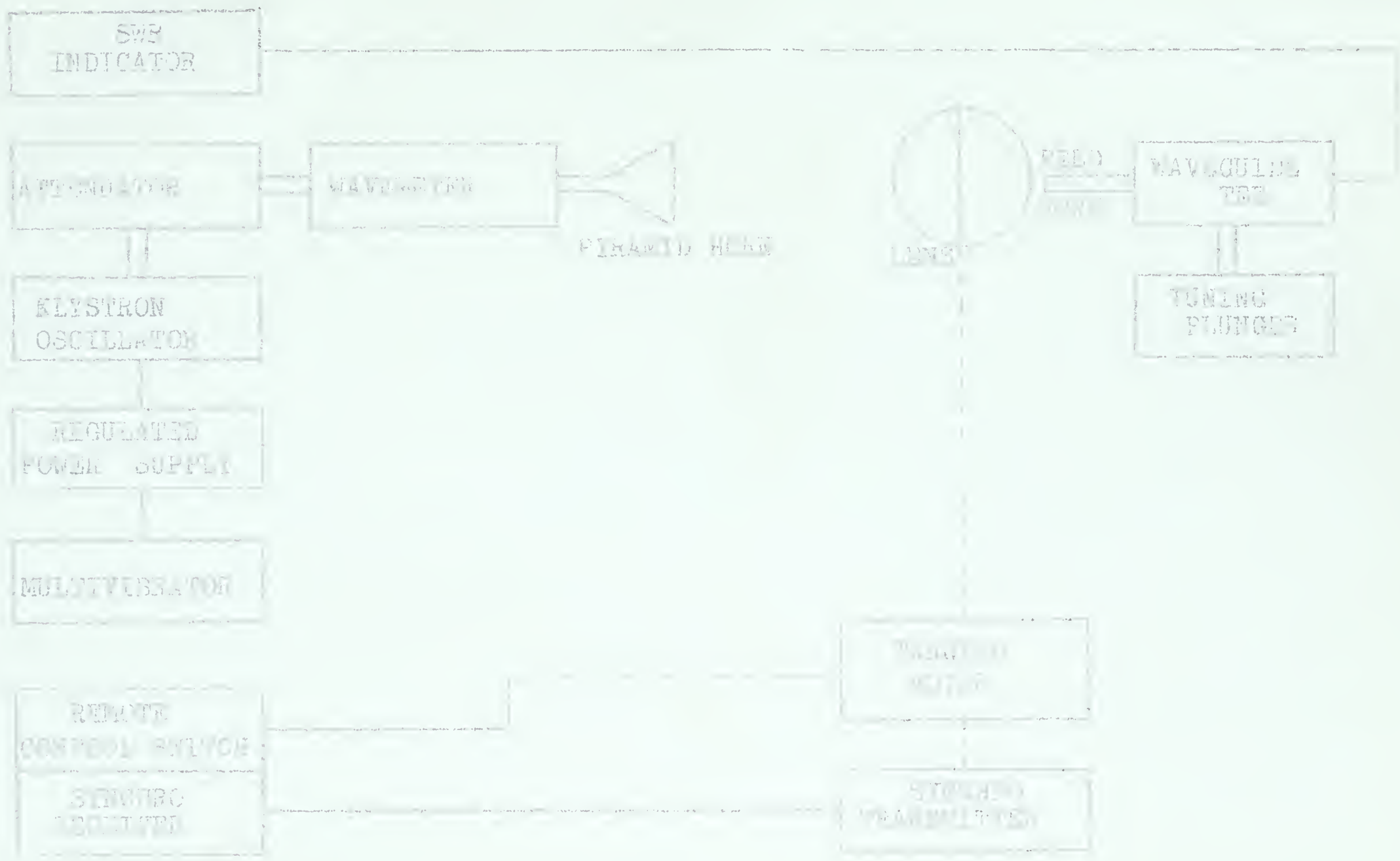
SWR
INDICATOR
ATTENUATOR
WAVEGUIDE
PYRAMID HEAD
KLYSTRON
OSCILLATOR
REGULATED
POWER SUPPLY
MODULATOR
REMOTE
CONTROL STATION
SERVICE
CONTROLS
WAVEGUIDE
TEE
TUNING
PLUNGER